Legacy-micropollutant contamination levels in major river basins based on findings from the Rhône Sediment Observatory

Hugo Delile, André-marie Dendievel, Anice Yari, Matthieu Masson, Cecile Miege, Brice Mourier, Marina Coquery

Legacy-micropollutant contamination levels in major river basins based on findings from the Rhône Sediment Observatory

Hugo Delile[1,2]*, André-Marie Dendievel[3], Anice Yari[1], Matthieu Masson[1], Cécile Miège[1], Brice Mourier[3], Marina Coquery[1]

[1]INRAE, UR RiverLy, 5 Rue de la Doua CS 20244, F-69625, Villeurbanne, France

[2]Univ. Lyon, CNRS, Archéorient, UMR 5133, Maison de l'Orient et de la Méditerranée, France

[3]Univ. Lyon, Université Claude Bernard Lyon 1, CNRS, ENTPE, UMR 5023 LEHNA, F-69518 Vaulx-en-Velin Cedex, France

*Corresponding author: hugo.delile@cnrs.fr

KEYWORDS: Micropollutant yields, Long-term monitoring program, Large river basins, Anthropogenic pressures, Persistent Organic Pollutants, Trace Metal Elements

Abstract

For more than half a century, chemical contamination has progressively spread to all the world's large river basins. Large river outlets integrate multiple anthropogenic pressures in watersheds, making them the largest source of sediment-bound contaminants to continental shelf areas. However, comparing particulate micropollutant contaminations between the large river basins is a challenging task, especially due to the scarcity of long-term river monitoring programs. Here we address this issue, with a focus on legacy particulate micropollutants (polychlorobiphenyls [PCBi], polycyclic aromatic hydrocarbons [PAHs], and trace metal elements [TME]) yields. For this purpose, we employed a bottom-up multiscale approach to chemical contamination in river basins that takes micropollutant yields measured in the Rhône River sub-basins (France) as a benchmark of other large river basins. Data on the Rhône River basin came from a unique 10-year-long monitoring program within the Rhône Sediment Observatory (OSR), and were compared to data gathered on 18 major worldwide river outlets.

The Rhône River basin is far cleaner now than a few decades ago, likely due to environmental regulations. At a wider spatial scale, our results depict an overall contamination gradient splitting the most heavily contaminated river basins, located in developing and industrializing low-to-middle-income countries, from the least contaminated rivers located in developed high-income countries. We argue that chemical contamination levels of large river basins depend on their stage of economic development.

1. INTRODUCTION

For more than five decades, freshwaters worldwide have experienced large-scale chemical deterioration, especially by legacy pollutants, to the extent that water quality concerns have become a major challenge for humanity in the twenty-first century (Meybeck and Helmer, 1989; Schwarzenbach et al., 2010; UNEP-DHI and UNEP, 2016; Damania et al., 2019). As a result, over the last ten years, this chemical contamination issue has become part of a broader concept called "planetary boundaries". These environmental limits define "a safe operating space for humanity" through nine processes regulating the stability and resilience of the Earth system (Rockström et al., 2009). Nonetheless, chemical contamination remains unquantified within the framework of this concept (Steffen et al., 2015; Lade et al., 2020). The general lack of large-scale and long-term monitoring programs limits efforts to assess the chemical risk at local and regional scales (e.g. Schwarzenbach et al., 2006; Steffen et al., 2015; Malaj et al., 2014), and is therefore a bottleneck to global-level assessment of chemical contamination in freshwaters. In a recent attempt to assess global river contamination, water quality was dealt with solely via two main categories of pollutants: nutrients (nitrogen and phosphorous) and pathogens (untreated human waste; UNEP-DHI and UNEP, 2016; Best, 2019; Damania et al., 2019). However, more than 140,000 different chemicals have been synthesized since the mid-twentieth century (Landrigan et al., 2018), which further complicates efforts to produce a global-level assessment of chemical contamination in rivers.

Rivers, floodplains, and watersheds in general have all helped to support the development of human societies, especially by supplying natural resources required for agro-pastoral, industrial, urban, domestic and mining activities (e.g. Macklin and Lewin, 2015; Vianello, 2015; UNEP-DHI and UNEP, 2016; Best, 2019). In return, these anthropogenic activities have released land-based organic and inorganic micropollutants into nearby rivers, which then carried pollutants downstream to coastal plains (Meybeck, 2003; Schwarzenbach et al., 2006). As a result, rivers ensure source-to-sink transport of sediment-bound micropollutants (Meybeck and Helmer, 1989; Gioia et al., 2011; Gómez-Gutiérrez et al., 2006; Wang et al., 2007; Liu et al., 2009; Delile et al., 2020). For these reasons, large river basin outlets can be seen as integrators of multiple anthropogenic pressures in watersheds, and thus as a proxy for assessing the global distribution of chemical contamination of upstream freshwaters.

Here we chose to focus on micropollutants that (i) remain a global concern due to their ubiquity at worldwide scale and (ii) are preferentially transported on particles. In this respect, suspended particulate matter (SPM) provides an integrated signal of particle-bound micropollutant concentrations (Schwientek et al., 2013; Masson et al., 2018; Rügner et al., 2019). The studied sediment-bound legacy contaminants are persistent organic pollutants (POPs: polychlorobiphenyls [PCBi] and polycyclic aromatic hydrocarbons [PAHs]) and trace metal elements (TME: arsenic - As, cadmium - Cd, cobalt - Co, chromium - Cr, copper - Cu, mercury - Hg, nickel - Ni, lead - Pb and zinc - Zn), all of which are considered as global, legacy contaminants (Schwarzenbach et al., 2010).

These contaminants are also known to be particularly harmful because of their toxic, persistent, bioaccumulative, and/or lipophilic properties (Schwarzenbach et al., 2010). Their main impacts on aquatic environments are loss of biodiversity and impairment of ecosystem services (Beketov et al., 2013; Malaj et al., 2014; Rasmussen et al., 2012; Schäfer et al., 2013).

Their risks to human and animal health are primarily related to their carcinogenicity and neurotoxic, genotoxic, and immunotoxic effects (Lauby-Secretan et al., 2013).

The main goal of this study is to assess releases of particle-bound chemicals by some of the large river basins spread across five of continents using specific fluxes of legacy organic and inorganic micropollutants, which we call "micropollutant yields". We compared contamination levels among the world's large river basins (Europe: Rhône, Garonne, Loire, Seine, Volga, Danube, Elbe, and Rhine; Asia: Pearl [Zhujiang], Liao, Yangtze [Changjiang], Yellow [Huang He], Mekong, and Ganges-Brahmaputra; North America: Mississippi, Colorado, and St. Lawrence; South America: Amazon; Africa: Niger) based on a bottom-up multiscale river basins approach. In this bottom-up approach, we use a comprehensive and unparalled monitoring from one river basin (i.e., a benchmark) to provide an assessment of the use of micropollutant yields as an indicator of river basin contamination. We used the medium-sized Rhône River basin as a benchmark because it has highly resolved (spatial and temporal) data on particulate micropollutant concentrations, fluxes and yields collected over a 10-year-long monitoring program as part of the Rhône Sediment Observatory (OSR) (Poulier et al., 2019; Delile et al., 2020). We also investigated the relationship between magnitude of micropollutant contaminations and economic stages of development (Meybeck and Helmer, 1989; Shafik, 1994; Panayotou, 2000).

2. DESIGNING A BOTTOM-UP MULTISCALE APPROACH TO ASSESS THE RIVER-BASIN CONTAMINATION

To assess contamination levels in major river basins spread around the globe, we developed a bottom-up multiscale approach using particulate micropollutant yields as a consistent proxy for inter-basin comparison of micropollutants contamination. Particulate micropollutant yields were estimated as the total inter-annual volume of particulate micropollutant fluxes (kg or t

yr^{-1}) discharged at the river outlets weighted by the size (km²) of the river watersheds (Meybeck and Helmer, 1989; Mäkelä and Meybeck, 1996; Babut et al., 2016; Delile et al., 2020).

We started by analyzing the contamination of the sub-basins of the Rhône River to assess the spatial representativeness of this proxy at a larger scale, i.e. the whole Rhône River basin. We then extrapolated this information on micropollutants contamination of the Rhône River basin to other large French river basins (Loire, Garonne, and Seine) and major continental river basins (Europe, Asia, North and South America, and Africa) to assess country- to continental-scale freshwater chemical contamination. Finally, we performed an inter-continent comparison of chemical contamination levels in large river basins.

This bottom-up multiscale river basins approach also helped us to unravel the major drivers of micropollutant yields, especially sensitivity to SPM fluxes and land-use. Land cover data on the Rhône River basin and its main sub-basins were derived from the Corine Land Cover (CLC) year 2018-version database (EEA, 2020) and classified into eight major categories (forests, agricultural land, shrub and/or grassy vegetation, bare areas, urban areas, industrial and commercial areas, water bodies, and others). These categories were merged from the 44 categories available in the CLC. One of the most important issues addressed in this study is the role played by the successive economic stages of development in shaping the magnitude of legacy micropollutant-based contamination of the large river basins. Here again, the long-term monitoring of the Rhône River basin enabled us to assess pluri-decadal temporal trends in micropollutant pollution. We then compared these trends against the historical pattern of economic development in the Rhône River basin since the 1980s. Finally, feedbacks identified for the Rhône River basin allowed us to explore the interrelationship between economic development stage and pollution magnitude at the scale of large river basins.

The several temporal scales required by the bottom-up multiscale approach implied referring to three specific chronological series:

- The intra-decadal trends refer to the 2008–2019 period based on the dataset gathered monthly or every two weeks by the OSR monitoring program. Trends are therefore computed at a high temporal resolution (bi-monthly to monthly) but over a relatively short period (around one decade);
- The inter-decadal trends refer to the 1980s–2010s period and a comparison of one decade to the next. Trends are therefore computed at a low temporal resolution (one decade) but over a relatively long period (four decades);
- The inter-annual temporal resolution refers to the average of each individual year for the 2008–2018 period for the Rhône River basin and the 2000-2020 period for the large river basins. We use the inter-annual data to address spatial rather than temporal trends.

3. STUDY AREA

3.1. Monitoring context of the Rhône River basin

The Rhône River is the largest single source of freshwater (~18% of the total inputs) (UNEP/MAP, 2003; Antonelli et al., 2008; Ludwig et al., 2009) and particulate matter (Qi et al., 2014; Antonelli et al., 2008; Syvitski and Kettner, 2007) to the Mediterranean Sea. Water and sediment are released by a complex hydrological regime, which comprises a tri-modal distribution over the year, including snow and glacier melting (Isère River and the Upper Rhône River), an oceanic pluvial regime (Saône River), and a Mediterranean component (Durance River) (Pardé, 1925; Bravard and Clemens, 2008). The geological contrast of the Rhône River basin is summarized by both its old western Hercynian crustal segments (240 Ma and older) of the Massif Central, and its young eastern Alpine mountains (30–120 Ma) (Blichert-Toft et al., 2016). Readers seeking further details on the geological and hydrological features of the Rhône River basin are invited to see extensive description recently published by Dendievel et al. (2020b).

Since 2009, the Rhône Sediment Observatory (OSR) has become the most extended and in-depth sedimentary monitoring network in France, featuring integrative or high-frequency measurements throughout the ~100,000 km² Rhône River basin (Fig. 1 A) of 1) particulate organic and inorganic micropollutant concentrations, 2) SPM, and 3) water discharge (Poulier et al., 2019). The monitoring network includes several sampling stations distributed along the Rhône River and at the outlets of its main tributaries, from Lake Geneva to the Mediterranean Sea (Fig. 1A). Two main stations are located directly on the French part of the Rhône River at Jons and Arles/Beaucaire, and further secondary stations have been set up on its main tributaries just upstream of their confluence with the Rhône River (Arve, Fier, Saône, Gier, Isère, Drôme, Durance, Ardèche and Gardon Rivers) (Le Bescond et al., 2018; Thollet et al., 2021). We have used data from the 10-year-long OSR to accurately quantify the inter-annual (2008–2018) average particulate micropollutant fluxes discharged into the Mediterranean Sea, decipher their seasonal dynamics within the Rhône River catchment, and estimate the specific contributions of the main tributaries (Delile et al., 2020). In this study, we focused on stations in the Upper Rhône River (Jons), the Saône River, the Gier River, the Isère River, the Durance River, and the Rhône River outlet (Arles/Beaucaire) (Fig. 1A and Tab. S1), as they have the longest monitoring history (Poulier et al., 2019). The six stations cover 80% of the watershed area (~96,500 km^2) (Fig. 1 and Tab. S1).

3.2. Defining the major worldwide river basins investigated

There has been extensive discussion in the scientific literature on which indicator best describes river size (river length, drainage basin area, water discharge, etc.; Best, 2019). The "world's large rivers" considered in this paper are those that have a river basin area greater than 100,000 km^2 (Meybeck and Helmer, 1989), and that host large populations (Tab. 1). There are more than 250 rivers worldwide with drainage basins larger than 100,000 km². However, by considering the sum of the population hosted in each of the 19 river basins considered in this study (□ 2

billion inhab.) and their respective annual sediment flux discharges (□ 4,000 Mt yr^{-1}), the 19 basins taken together account for around □ 30% of the global population (□ 7 billion inhab.) and fluvial sediment discharge (13,000 Mt yr^{-1}) (Syvitski et al., 2005; Syvitski and Kettner, 2011; Bravard, 2018) (Tab. 1). This selection of large rivers was also based on the availability of data on the sediment fluxes and concentrations of the targeted particulate micropollutants (PCB, PAH, and TME) at the river outlets, and on the selected economic indicators (population, urbanization, Gross Domestic Product [GDP], dams) (data sources shown in Tab. 1).

4. METHODS

In this section, we define the study area, the datasets used to compute the temporal trends of the Rhône River basin and the inter-annual particulate micropollutant yields of the large river basins.

4.1. Assessment of temporal trends in particulate micropollutant concentrations and fluxes at the Rhône River outlet

We describe here the methodology used to assess temporal trends (1980s-2010s) in particulate micropollutant concentrations ($C_{micropol}$) and fluxes ($F_{micropol}$), and SPM fluxes (F_{SPM}) at the Rhône River outlet. Sub-section 4.1.1. describes the data and statistical tests used to assess the temporal evolution in chemical water quality at the Rhône River outlet at inter-decadal (1980s–2010s period) and intra-decadal (2008–2019 period) resolution (Tab. 2). Then, in sub-section 4.1.2., we describe the methodology used to calculate the inter-decadal micropollutant concentrations and fluxes (1980s–2010s). In section 2.4, we describe the inter-annual micropollutant yields calculated over the 2008–2018 period.

4.1.1. River sediment matrices used and statistical tests

The inter- and intra-decadal resolution of temporal trends in particulate micropollutant concentrations and fluxes at the Rhône River outlet since the 1980s is based on two datasets (Tab. 2 and Fig. S1):

- prior to 2008–2010, TME, PAHs and PCBi data came from research labs and monitoring agencies studying deposited sediments, i.e. bed and flood deposits, and sediment cores;
- after 2008–2010, TME, PAHs and PCBi data came primarily from SPM measured under the OSR monitoring program. A small amount of data acquired on deposited sediments was also used to build a composite record for the 2010–2019 period.

The dataset used to assess inter-decadal trends includes several types of sediment matrices (Tab. 2) that are likely to affect micropollutant concentrations (effect of grain-size distribution and/or organic matter concentrations). For this reason, in figure S1, we compared micropollutant concentrations between suspended (SPM) and deposited sediments (including bed and flood deposits, and sediment cores) for the 2010–2019 period. Overall, organic micropollutant concentrations were □ 25% lower in SPM than in deposited sediments, whereas TME were 30% to 100% higher in SPM. Even though these differences are not negligible, concentrations remain similar in magnitude and were used for the assessment of the inter-decadal trends. However, the dataset used for the assessment of intra-decadal trends was exclusively from SPM sediments (Tab. 2), since at this fine temporal scale, mixing various sediment matrices would undermine the results.

Micropollutant concentrations data were gathered from the lower part of the Rhône River (Arles/Beaucaire station, i.e. 120 kilometers from the Rhône River outlet) for TME (Cd, Cr, Cu, Hg, Ni, Pb and Zn), 7 indicator PCBi (congeners 28, 52, 101, 118, 138, 153, and 180; noted Σ_7PCB, and 12 priority PAHs (anthracene, benz[a]anthracene, benzo[a]pyrene, benzo[b]fluoranthene, benzo[ghi]perylene, benzo[k]fluoranthene, chrysene, dibenz[a,h]anthracene, fluoranthene, indeno[1,2,3-cd]pyrene, phenanthrene, pyrene; denoted with the abbreviation Σ_{12}PAH). All of these data were produced by monitoring authorities (the Rhône–Mediterranean–Corsica water agency) and the OSR monitoring program. Our database

includes several particulate matrices, i.e. bed and flood deposits, SPM and sediment cores. Additional sediment core data came from various research labs (Tab. 2).

More specifically, PAH data from bed and flood sediments over the period 1994–1997 were available from the Rhône–Mediterranean–Corsica water agency (data source: http://www.naiades.eaufrance.fr) (Tab. 2), whereas PAH data for SPM come from the OSR dataset over the period 2011–2016 (Delile et al., 2020; Thollet et al., 2021). The TME and Σ_7PCB analyses are available since the 1980s (Tab. 2) based on data for sediment cores and bed and flood deposits (see Dendievel et al., 2020a,b for details on the data, stations and methods used). Over the periods 2011–2018 for TME and 2008–2017 for PCBi, we only used SPM data from the OSR dataset (Delile et al., 2020; Thollet et al., 2021). Arsenic (As) and cobalt (Co) were only measured since the 2010s in the OSR program and were not measured in previous decades (Tab. 2).

To decipher temporal trends in micropollutant concentrations and mean monthly water discharges data during the past decade, we used HYPE software for trends identification of time-series (Croiset and Lopez, 2013). We used the non-parametric Mann-Kendall test for identifying monotonic trends over the entire duration of time-series because micropollutant concentrations data were not normally-distributed. We used the modified Mann-Kendall test (Hamed and Rao, 1998) because (i) each micropollutant data time-serie has more than 40 analyses and (ii) the test is valid for assessment of autocorrelation in time-series data. Only the statistically significant temporal trends (p-value < 0.05) over to the total length of the time-series are presented. Furthermore, two-steps structural break tests were performed for each micropollutant time-series. Firstly, we applied the non-parametric Pettitt's test (Pettitt, 1979) derived from the Mann-Whitney test to detect a change of average in time-series. The tipping point was considered statistically significant when the p-value of the test was less than 5%. Secondly, we used the non-parametric Darken's test (Darken, 1999; Darken et al., 2000) to

identify a trend reversal in time-series consisting in a change of the sign of a slope. Trend reversal Darken test compares the Kendall's tau for two sections in time-series. If the p-value is less than 5%, then the micropollutant series includes a significant trend reversal, and the break dates are determined.

4.1.2. Calculation of temporal trends in particulate micropollutant concentrations and fluxes

The calculation of inter-decadal particulate micropollutant fluxes at the Rhône River outlet is summarized below in three steps.

Firstly, TME concentrations in sediment cores were measured using an *Aqua Regia* digestion (hydrochloric acid - 3N HCl and nitric acid - HNO_3) (Dendievel et al., 2020c), and bed, flood and SPM sediment samples were analyzed using a total extraction (HCl, HNO_3, H_2O_2 and hydrofluoridric acid - HF) (see Delile et al., 2020 for the detailed analytical procedure). Thus, in order to combine and compare these data, TME concentrations from sediment cores were corrected according to the relationships between these two types of extractions as proposed by Dendievel et al. (2020c). From these legacy micropollutants datasets, we computed inter-decadal trends (1980s-2010s) for the particulate micropollutant concentrations.

Second, we reconstructed the inter-decadal SPM fluxes since the 1980s. We used the SPM data systematically measured under the OSR program since 2011, but a reconstruction was needed for the earlier periods without regular measurement. Thus, based on the known water discharge for each month (available at http://www.hydro.eaufrance.fr), the SPM concentrations (mg L^{-1}) and fluxes (Mt yr^{-1}) were reconstructed using the specific rating curves and equations published by Poulier et al. (2019) for the Rhône River.

Third, we calculated the inter-decadal micropollutant fluxes (1980s–2010s). These fluxes were computed by multiplying the SPM fluxes (step 2) by the decadal median of the micropollutant concentrations resulting from both monitoring series (from the Rhône–

Mediterranean–Corsica water agency on bed and flood sediments, and from the OSR monitoring program on SPM), and dated sediment cores (Tab. 2).

4.2. Assessment of the Rhône River basin's inter-annual micropollutant yields

The inter-annual micropollutant yields computed as specific micropollutant fluxes (g or kg km^{-2} yr^{-1}, i.e. the micropollutant fluxes weighted by the watershed size), provide an integrative estimation of the chemical contamination level of the river basin. First, to assess the inter-annual average micropollutant fluxes over the 2008–2018 period, we calculated the SPM fluxes as the product of hourly measured data on both water discharges and SPM concentrations at each station in the OSR (Fig. 1 and Tab. S1). Second, micropollutant fluxes were calculated by multiplying the SPM fluxes by monthly time-integrated and flow-proportional particulate micropollutant concentrations obtained from particle traps (Schulze et al., 2007; Masson et al., 2018; Poulier et al., 2019; Delile et al., 2020) or by a continuous flow centrifuge (for the Arles/Beaucaire station only). Masson et al. (2018) compared micropollutant concentrations measured by both SPM sampling methods at the Jons station (draining the Upper Rhône River basin, Fig. 1) and did not find statistically significant between-method differences, which suggests that these SPM sampling systems are comparable. Data for micropollutants with a quantification frequency (QF) < 50% were not considered in the present study (4 priority PAHs). For some other organic micropollutants (PCBi and PAHs), data that were below the limit of quantification (LOQ) were changed to LOQ/2 for calculation of micropollutant fluxes. Readers seeking further details on the micropollutant fluxes computation, and especially about the filling of non-monitored periods or gaps in the measurement time-series of both SPM and micropollutant concentrations and the estimation of flux uncertainties, are invited to see the extensive description by Delile et al. (2020). Third, the inter-annual particulate micropollutant fluxes at the mouth of the Rhône River (Arles/Beaucaire station) and its main tributaries (Saône River, Upper Rhône River, Gier River, Isère River and Durance River; Fig. 1 and Tab. S1) were

weighted by the corresponding watershed size to get the micropollutant yields (g or kg km^{-2} yr^{-1} for POPs or TME, respectively) at the Rhône River basin and sub-basin scales.

4.3. Assessment of the inter-annual micropollutants yields of the world's large river basins

To assess micropollutant yields, we estimated the annual sediment fluxes discharged at the outlet of the selected rivers. Accurate estimation of sediment fluxes remains a challenging issue (Mouyen et al., 2018; Poulier et al., 2019; Hackney et al. 2020), especially at global scale, because less than 10% of the river mouths worldwide have monitoring of sediment delivery (Syvitski et al., 2005; Bravard, 2018). In addition, *in-situ* sediment discharge measurements are highly uncertain (spatially sparse and temporally discontinuous data, different-measurement time frequencies, heterogeneous measuring techniques) (Mouyen et al., 2018). We therefore used the modeled annual fluvial sediment fluxes (Nienhuis et al., 2020) for all of the large rivers included in this study (Tab. 1). These data were produced using WBMSed (Cohen et al., 2013, 2014) and BQART (Kettner and Syvitski, 2008) methods. This approach using modelled estimates of sediment flux at the large river outlets appears particularly suitable for our study, since it catches the multiyear average sediment fluxes as well as inter-annual and intra-annual trends (Cohen et al., 2013).

Then, annual micropollutant fluxes were calculated by multiplying the sediment fluxes by the median concentration of each micropollutant (Fig. S2) for each river on the basis of sediment samples collected at the outlet of the rivers. Based on our homemade micropollutant concentrations database, Table S2 shows specific concentrations (median and range) of micropollutants (mg or µg kg^{-1} dry weight), inter-annual particulate micropollutant fluxes (kg or t yr^{-1}), yields (g or kg km^{-2} yr^{-1}) and per capita data (mg or g $inhab^{-1}$ yr^{-1}) for 19 large rivers spread among five continents. The references used to establish this database are detailed in Supplementary Text. All the data gathered on our homemade micropollutant concentrations

database come from sediment samples collected over the 2000–2020 period and refer to several sediment matrices including surface, bed and flood deposits, SPM, and sediment cores. Data sources (Supplementary Text) include data and scientific papers (e.g., Dendievel et al., 2020a,b, c), academic studies (e.g. Masson, 2007), databases of river monitoring surveys (e.g. OSR for the Rhône River, https://bdoh.irstea.fr/OBSERVATOIRE-DES-SEDIMENTS-DU-RHONE/; the IKSR-CIPR-ICBR program for the Rhine River, http://iksr.bafg.de/iksr/auswahl.asp?S=1; the HYBAM observatory for the Amazon River, http://www.ore-hybam.org), and institutional organizations (e.g. French water agencies, data source: http://www.naiades.eaufrance.fr). Our database contains sediment samples collected at the outlet of the rivers in order to get an integrative signal of the watershed. In addition, particular attention was paid to exclude sampling stations potentially affected by mixing with saline oceanic or estuarine waters. Regarding PAHs and PCBi, for each sample, we either directly compiled available data on the sum of the 16 priority PAHs (INERIS, 2005) and the sum of the 7 indicator PCBi congeners, or manually calculated these sums using available data on individual chemicals. The 16 priority PAHs are not systematically available in the scientific literature or other data sources: indeed, the number of priority PAHs initially measured ranges from 12 to 16 PAH. Consequently, results are shown as $\Sigma_{12\text{-}16}$PAH. For this reason, but also given the great diversity of the data collected and the resulting uncertainties in sediment flux estimates, the computed micropollutant yields of large river basins were classified according to 3 or 4 orders of magnitude. Thus, the spatial distribution of the $\Sigma_{12\text{-}16}$PAH yields, for instance, was divided in three order-of-magnitude classes, i.e. (1) 1–10, (2) 10–100 and (3) >100 g km^{-2} yr^{-1}.

5. RESULTS

We present in this section results on the temporal and spatial trends of contamination in the Rhône River basin and on the assessment of the relationship between the micropollutants yields and SPM yields of large river basins.

5.1. Temporal trends in the Rhône River basin contamination

5.1.1. Long-term trends in micropollutant contamination since the 1980s

Figure 2 shows the pluri-decadal trends in particulate micropollutant concentrations and fluxes and SPM fluxes during the last 40 years at the Rhône River outlet. Table 3 presents specific variations (in percent) of micropollutant concentrations and fluxes and SPM fluxes from one decade to the next, noted $\Delta C_{micropol}$, $\Delta F_{micropol}$ and ΔF_{SPM}, respectively. The general time–course of micropollutant concentrations and fluxes follows a similar decreasing trend between 1980s–1990s: -58% for $\Delta C_{\sum 7PCB}$ and -69% for $\Delta F_{\sum 7PCB}$, and -42% for mean ΔC_{TME} and -57% for mean ΔF_{TME}.

After the 1990s, the organic and inorganic micropollutant concentrations and fluxes follow distinct patterns. POPs continued to decline in similar and stable proportions, both in concentrations (1990s to 2010s, $\Delta C_{\sum 7PCB}$ □ -39%, and $\Delta C_{\sum 12PAH}$ □ -38% on average) and fluxes (1990s to 2010s, $\Delta F_{\sum 7PCB}$ □ -37%, and $\Delta F_{\sum 12PAH}$ □ -35% on average) (Fig. 2A-D and Tab. 3). The time–course of PCB and PAH fluxes over the period reproduces the same pattern as the concentrations. In contrast to the POPs, TME fluxes showed a similar pattern of change to the SPM flux trend. TME and SPM fluxes decreased significantly with similar rank order of magnitude between the 1990s–2000s (ΔF_{TME} □ -34% and ΔF_{SPM} □ -28%), whereas ΔC_{TME} decreased slightly (□ -8%) over the same period. Thereafter, TME and SPM fluxes increased sharply between 2000 and 2010s (ΔF_{TME} □ +21% and ΔF_{SPM} □ +44%) while ΔC_{TME} experienced a slight decline (□ -8%) (Fig. 2E-F and Tab. 3).

The relative weights of $C_{micropol}$ and F_{SPM} in $F_{micropol}$ variations from one decade to the next were assessed (see Tab. 3) by comparing (i) the decadal variations (in %) of inter-annual particulate micropollutant concentrations (ΔC) and fluxes (ΔF), and SPM flux and (ii) their respective correlation coefficients. We defined three micropollutant groups by assessing the

weight of $\Delta C_{micropol}$ and ΔF_{SPM} in $\Delta F_{micropol}$: (1) concentration-driven micropollutant fluxes for $\sum_7$PCB, $\sum_{12}$PAH, Cd, Cr and Hg (orange cells, and statistically significant correlation coefficients of $F_{micropol}$ vs. $C_{micropol}$ in Tab. 3), (2) SPM flux-driven micropollutant fluxes for Cu and Ni (grey cells, and statistically significant correlation coefficients of $F_{micropol}$ vs. F_{SPM} in Tab. 3), and (3) alternately concentration-driven and SPM flux-driven micropollutant fluxes for Pb and Zn (orange and grey cells, and statistically significant correlation coefficients of $F_{micropol}$ vs. $C_{micropol}$ and of $F_{micropol}$ vs. F_{SPM} in Tab. 3). According to Table 3, SPM flux-driven micropollutant fluxes switch to concentration-driven micropollutant fluxes when $\Delta C_{micropol}$ is higher than □ ± 30%. In other words, variations of micropollutant concentrations have to vary by more than 30% in order to affect micropollutant fluxes. Below this threshold, SPM fluxes primarily control micropollutants fluxes.

5.1.2. Short-term trends in micropollutant contamination over the past decade

Figure 3 shows the temporal evolution of particulate micropollutant concentrations at the Arles station (Rhône River outlet, Fig. 1) over the past decade (2010s). Mean monthly water discharges and associated temporal trends over the total length of the time-series are also shown in order to capture the relationship between the water discharge trends and the micropollutant concentrations trends. Overall, the results highlight three micropollutant trend groups: (1) increasing concentrations for As, Co, Cr, Ni and Zn, (2) decreasing concentrations for Σ_7PCB, and (3) no trend for Σ_{12}PAH, Cd, Cu, Hg and Pb (Fig. 3). Given that the mean monthly water discharge does not show statistically significant temporal trends, it cannot lead to an increase or decrease in micropollutant concentration trends.

The comparison between the increase in annual rates of TME concentrations (red values in Fig. 3) of the first group (As, Co, Cr, Ni and Zn) and their respective median value (Tab. S2) indicates an average annual rate of increase of 7% per year.

The second trend group (2) concerns Σ_7PCB concentrations, which over the total length of the time-series (2008-2016) decreased at a mean annual rate of 1.4 µg kg^{-1} (i.e. -9% per year; Fig. 3). This trend is in line with the general pattern of decreasing PCB contamination of the Rhône River waters that began in the 1990s (Desmet et al., 2012; Mourier et al., 2014; Babut et al., 2016; Liber et al., 2019; Dendievel et al., 2020a) (Fig. 2A). Nonetheless, the trend showed a change-point in October 2013, with a slight increase in PCB concentrations of about +1.6 µg kg^{-1} per year (i.e. +9%) (Fig. 3).

5.2. Spatial trend in Rhône River basin contamination

Figure 4 is a map of the particulate micropollutants yields of the whole Rhône River basin and its main sub-basins. It shows a sharp contrast between a less contaminated area in the North (Saône River and Upper Rhône River basins) and a more contaminated area in the South (Isère River, Gier River and Durance River basins). This contrast appears more clearly for TME yields, which have a spatial distribution pattern that matches the features of intra-basin SPM yields (Fig. 4). As a result, TME yields in the different tributaries seem to be sensitive to variation in SPM yields. The SPM yields in the Rhône River basin come mainly from the Isère and Durance river basins, since they are known to be the largest suppliers of the inter-annual SPM flux discharged into the Mediterranean Sea from the Rhône River outlet. Each of these two tributaries accounts for 31% of the total inter-annual SPM flux of the Rhône River, while the Upper Rhône River, Saône River and Gier River account for 11%, 6%, and 0.1%, respectively (Delile et al., 2020).

Figure 5 is a Principal Component Analysis (see details on the PCA method in the Supplementary Text) combining the micropollutants yields, population density and land use of each station (Fig. 1B). The first principal component (F1 ~ 56%) results from the contribution of all micropollutants yields, meaning that F1 tracks the overall contamination level. However,

the contribution of mean TME yields to the F1 component (7.5%) is twice as large as the contribution of organic micropollutants (2.7%). Organic micropollutants are more involved in the F2 positive values, since PAH and PCB yields contribute on average about 8% to the F2 component (only 2.5% for mean TME contribution). The F2 axis shows a striking contrast between anthropogenic land use (positive values) as agricultural lands, urban areas and industrial and commercial areas (ICA) on one side and natural land use (forests, bare, and shrub/vegetation) (negative values) on the other (Fig. 5). Population density is highly correlated to urban areas and ICA ($R > 0.93$ and 0.89, respectively; p-value < 0.05). Based on the F2 component, TME yields divide into two groups: first, a natural land use-related TME group with Cr, Co, Ni and Hg, and a second anthropogenic land use-related TME group with As, Pb, Zn, Cd and Cu (Fig. 5). In addition, the first TME group is significantly correlated with SPM fluxes (R values 0.93–0.98; p-value < 0.05), which is not the case for the second group (R values 0.48–0.68; p-value > 0.05). The location of the river stations into the PCA differentiates the northern and southern areas of the Rhône River basin: the Upper Rhône and Saône rivers in the north showing the lowest micropollutant yields, and the Isère and Durance rivers in the south characterized by natural land use and SPM flux-bound TME yields. The Gier River appears to be the most contaminated basin, especially for organic micropollutants yields (Fig. 4), and also the most impacted by anthropogenic land use (Figs.1 and 5).

5.3. Assessment of the relationship between the micropollutant yields and SPM yields of the large river basins

Building upon our findings from the Rhône River basin on the main patterns of micropollutant yields, we next extrapolated that knowledge of SPM fluxes to assess micropollutant yield signal of the large river basins. The maps of micropollutant yields show that some TME yields follow spatial trends of SPM yields (Fig. S3), whereas PAH and PCB yields seem unconstrained by SPM yields (Fig. 6). River basins in high-income countries (i.e. Europe and North America)

show the lowest SPM yields (< 66 t km² yr^{-1}) (except for the Rhine River basin), while river basins in low-income countries (i.e. Asia and South America) show the highest SPM yields (> 100 t km² yr^{-1}) (except for the Niger River basin) (Figs. 6 and S3, and Tab. 1).

The potential control of SPM fluxes on micropollutant yields was assessed through the correlation circle of the PCA (Fig. 7A, see details on the PCA method in the Supplementary Text) and the correlation matrices between micropollutant and SPM yields (Tab. S3), and between micropollutant yields and median concentrations (Tab. S4). We identified three groups of micropollutant yields:

1) Anthropogenic activity-driven PCB, PAH, Cd and Hg yields: uncorrelated with SPM yields (R □ 0.15-0.40, p-value > 0.05), and positively correlated to their median concentrations (R □ 0.6-0.8, p-value < 0.05);
2) SPM flux-driven Co, Cr, Ni and Cu yields: positively correlated to SPM yields (R □ 0.8-1, p-value < 0.05), and uncorrelated with their median concentrations (R □ 0.2-0.3, p-value > 0.05);
3) Anthropogenic activity/SPM flux-driven As, Zn and Pb yields: positively correlated to SPM yields (R □ 0.5-0.8, p-value < 0.05) and to their median concentrations (R □ 0.5-0.6, p-value < 0.05).

6. DISCUSSION

6.1. Insights from the bottom-up multiscale approach to assess the river-basin contamination

The assessment of the Rhône River's intra-basin contamination has shown a striking spatial heterogeneity between the northern and southern areas of the Rhône River basin. For instance, except for Zn, the first group of TME concentrations (As, Co, Cr, Ni and Zn) of the Rhône River basin matches the specific chemical fingerprint of the Isère River's SPM (Delile et al., 2020). We can therefore assume a process of enhanced soil erosion in specific Isère River sub-

basins on Ni, Co and Cr element-rich geological basements, leading to increasing concentrations of these TME over the past decade (2010s). However, only additional TME geochemical tracing methods, such as Pb, Cu and Zn isotopic fingerprinting techniques (Bird, 2011) or geochemical fingerprinting (Bégorre et al., 2021; Dabrin et al., 2021), could capture specific sources of TME in sediments. This heterogeneous pattern of the micropollutant yields of the Rhône River basin suggests that calculated micropollutants yields of the large river basins need to be considered with caution, in terms of the sources of the chemical fluxes. Such fluxes should not be considered as uniformly deposited over the entire surface of the river basins. Our reconstructions of the temporal trends of particulate micropollutant concentrations and fluxes at the Rhône River outlet since the 1980s show that micropollutant concentrations have to vary by more than 30% to affect micropollutant fluxes. As a result, this threshold defines the switch from SPM flux-driven to anthropogenic pressure-driven micropollutant yields. Applied to the other 18 large river basins worldwide, this balance between micropollutant concentrations and SPM fluxes suggests a progressive anthropogenic origin of the micropollutant yields as follows: (i) SPM flux-driven Co, Cr, Ni and Cu yields, (ii) anthropogenic activity and SPM flux-driven As, Zn and Pb yields, and (iii) anthropogenic activity-driven PCB, PAH, Cd and Hg yields.

It is striking to note that these large river basins-bound micropollutant yield groups are close to those identified in the Rhône River sub-basins since PCB, PAH, As, Pb, Zn, Cd and Cu yields are related to their contamination level, while Cr, Co, Ni and Hg yields are more related to their SPM yields. Only Hg and Cu yields do not belong to the same group. This is a key point. We argue that the diversity of the geological basements of the Rhône River sub-basins captured in Rhône Sediment Observatory data is the decisive factor for explaining this distinction between Hg and Cu yields.

As a result, regarding TME, the lack of geochemical background data for each river basin is a significant barrier to considering TME yields as a consistent proxy for assessing river basin

contamination. Indeed, as it stands, TME yields reflect a mixture comprising both the TME fraction coming from the local geological environment and TME fraction from the anthropogenic activity. Therefore, TME yields would be more suitable to track anthropogenic contamination of river basins if local geological effects on TME yields could be removed. Nevertheless, the clustering of TME demonstrates that the proportion of natural and anthropogenic inputs is not the same for all TME. Indeed, at the worldwide river basins scale, the anthropogenic source is the dominant contributor to Hg and Cd whereas the natural source is the dominant contributor to Ni, Co, Cr and Cu. The Rhône River monitoring network data shows the tipping-point switch from a predominantly natural to anthropogenic TME yields requires TME concentrations that are □ 30% higher than the local geochemical backgrounds.

6.2. Role of economic development on the global distribution of micropollutants yields

Considering all micropollutant yields, the distribution of the large river basins within the PCA defines three statistically-based mixing lines showing a gradient of overall contamination level from the least contaminated river basins in the bottom-left corner of the graph up to the most contaminated river basins in the upper-right part of the graph (Fig. 7B). The slope mixing lines depend of the relative weight between the anthropogenic origin of the micropollutant yields (Group 1-based mixing line) and the contribution of SPM fluxes to micropollutant yields (Groups 1 + 2 +3-based mixing line). The mixing lines split river basins into two groups: the most contaminated rivers located in developing countries (Asia and South America), and the least contaminated rivers located in developed countries (Europe and North America).

Based on the long-term trends of the Rhône River basin contamination, it appears that the overall chemical contamination level during the 1980s was similar to that currently observed in countries undergoing economic transition. According to previous works, the highest contamination levels, tied to the developing low-to-middle-income countries, result from

increasing demand for both energy required for petroleum-powered vehicles and electricity generation and natural resources (e.g., mining) or else from deforestation due to intensive agriculture (Schwarzenbach et al., 2010; Landrigan et al., 2018). This growing demand for energy and natural resources is driven by uncontrolled growth of cities and large-scale urbanization in these countries (Wilkinson et al., 2007; UNESCO, 2009; Shen et al., 2013).

The environmental quality improvement of the Rhône River basin during the 2010s is apparent as a leftward shift in Figure 8 towards the cluster of less-contaminated rivers. This substantial decline since the 1980s is part of a global decline in POPs (Breivik et al., 2002a,b and 2007 for PCB; Shen et al., 2011, 2013 for PAH) and TME releases (McConnell et al., 2019; Legrand et al., 2020). This decline may result from national (see French regulation timeline for PCBi in Fig. 2) and international implementations of environmental regulations (e.g. PCBi listed in the Stockholm Convention [UNEP, 2001] and PAHs in the Aarhus Protocol on Persistent Organic Pollutants [United Nations, 1998]) in many developed countries (Miller and Orbock Miller, 2007). Indeed, other studies have shown that the lower contamination level of the river basins located in developed countries results from (i) efforts to mitigate industrial, municipal and household wastewaters, (ii) the commissioning of sanitation and water supply infrastructures, and (iii) national and international environmental regulations on emissions control and the use of chemical products (UNESCO, 2009; Schwarzenbach et al., 2010; UNEP-DHI and UNEP, 2016; Landrigan et al., 2018; Damania et al., 2019).

This general model seems to show an environmental quality improvement depending on successive economic stages of development. Such a trend fits rather well with the theoretical framework of the Environmental Kuznets Curve (EKC) (Grossman and Krueger, 1991, 1995; Shafik and Bandyopadhyay, 1992). According to EKC theory, this relationship, which is assumed to take the form of an inverted U-shape curve, comes from a period of environmentally damaging economic growth followed by improvement in environmental quality as per capita

income and/or GDP rises. However, this theory has been criticized due to, for example, the unsuitable statistical analyses of time-series (Stern et al., 1996; Stern, 2004) or the environmental and economic activity indicators on which it is based (Dinda, 2004).

6.3. Comparison of the contamination levels in the world's large river basins

The observed relationship between country income level and SPM yield derives from well-known anthropogenic stresses such as agriculture-induced deforestation and river damming (Syvitski and Kettner, 2011; Bravard, 2018; Nienhuis et al., 2020).

Polycyclic aromatic hydrocarbons and TME yields mapping well depict the relevance of consumption of natural resources and energy for the economic development of our modern societies (Figs. 6 and S3). In both cases, the highest micropollutant yields of Asian countries (Figs. 6 and 8) are consistent with their atmospheric micropollutant emissions, since they contribute around 50% of the global $\sum_{16}$PAH (Shen et al., 2013) and TME emissions (Pacyna and Pacyna, 2001). It has been estimated that almost two thirds of the global $\sum_{16}$PAH emissions come from residential/commercial burning of biomass, and this source accounts for about 80% of emissions from South-East Asia (Shen et al., 2013). As underlined above, recent surging urbanization is considered as the main driver of this high PAH contamination in developing countries, because it results from extensive use of biomass for cooking and heating but also from petroleum consumption by road vehicles (Shen et al., 2011, 2013). River basins in Western Europe and North America show lower PAH yields (Figs. 6 and 8) thanks to the implementation of emissions reduction technologies (Shen et al., 2011, 2013) and a series of legislative policies in force since the 1970s, first with the 1979 Convention on Long-Range Transboundary Air Pollution (CLRTAP) (UNECE, 1979) and then the Aarhus Protocol on POPs (United Nations, 1998). The implementation of this regulatory framework has brought about a sharp decrease in $\sum_{12}$PAH yields in the Rhône River basin, from 100.5 g km^{-2} yr^{-1} in the 1990s to 34.6 g km^{-2} yr^{-1} in the 2010s. However, the Rhine and Elbe river basins show similar PAH yield levels to those

of Asian countries. The heavy industrial legacy of the Rhine and Elbe river basins (Heise et al., 2004; Förstner et al., 2004) could explain the high PAH contamination of these areas.

The spatial distribution pattern of TME yields is broadly similar to that of PAH, with the highest levels found in Asia, followed by river basins in Europe and North America. However, the Amazon River basin shows an equal if not higher level of TME contamination than river basins in Europe and North America (Figs. 6 and 8). Once again, this pattern is consistent with worldwide TME emissions estimates, since Asia accounts for between 40% and 60% of the total depending on the TME, followed by Europe, North America and South America which contribute between 10% and 20% depending on the TME (Pacyna and Pacyna, 2001; Streets et al., 2017; Kubier et al., 2019). The two main sources of Hg, Cd, As, Zn, Cu, and Ni contamination are non-ferrous metal production and non-vehicle fossil fuel combustion (Pacyna and Pacyna, 2001; Streets et al., 2017). For example, during the 1990s, gold mining in the Brazilian Amazon released around 130 t of Hg into the environment every year, of which about half of that amount reached surface waters (Pfeiffer et al., 1993; Lacerda and Salomons, 1998). By adding the other minor anthropogenic Hg sources (e.g. chemicals manufacturing, electrical and measuring equipment, Cu, Zn and Pb smelting, silver (Ag) production, coal and oil combustion, etc.), the calculated Hg emission yield of 11 g km^{-2} yr^{-1} is close to our appraisal of 12 g km^{-2} yr^{-1} (Table S2) and to other estimates, such as 9.3 g km^{-2} yr^{-1} (Fostier et al., 2000) or 7-17 g km^{-2} yr^{-1} (Roulet et al., 1999) for the Amazon River basin. This comparison shows that annual Hg yields derived from atmospheric emission and river outlet-bound particulate fluxes are able to accurately track the magnitude of river basin contamination.

Finally, the spatial distribution of the PCBs yields over the large river basins is more homogeneous than the other micropollutant yields, mainly because river basins in Asian countries do not have the highest contamination levels (PCBi yields □ 0.1 to 10 g km^{-2} yr^{-1}), which are of the same order of magnitude as that of river basins of the developed countries

(PCBi yields □ <0.1 to 10 g km^{-2} yr^{-1}; Figs. 6 and 8). This pattern is in line with the global pattern of PCB production and usage, which occurred mainly in North America and Europe (Breivik et al., 2002a; Desforges et al., 2018), while Asian countries, especially China, had only used PCB for a relatively short period (1965-1974) before they were banned. Only the South-Eastern coast of China has been significantly impacted (Xu et al., 2000; Mai et al.; 2005: Xing et al., 2011).

Our assessment is limited by particulate micropollutant fluxes that originate from the remobilization of contaminated sediments stored in rivers. For instance, the slight increase in PCB concentrations since 2013 at the Rhône River outlet could result from a potential remobilization of highly PCB-contaminated legacy sediments trapped within the alluvial margins leading to the persistence of PCBi in the Rhône River waters (Babut et al., 2016; Liber et al., 2019; Poulier et al., 2019; Delile et al., 2020). Legacy contaminants reintroduced into the river by physical processes (dam failure, greater flooding due to climate change, river restoration programs, etc.) (Noyes et al., 2009; Eschbach et al., 2018; Cornwall, 2020) and/or chemical processes (increasing solubility of some micropollutants; Stigliani, 1991; Schwartzman et al. 2010) are likely to confound the relationship between economic development phases and freshwater quality due to lag times (decadal to millennial time scales). Legacy contaminated sediments along the river continuum pertain to the issue of (i) contaminant residence times along river corridors (Pizzuto, 2014; Sutfin and Wohl, 2019; Wohl, 2015, 2019), (ii) total time for contaminant transfer to river outlets, and (iii) the theoretical decontamination time of a river basin (Singer et al., 2013; Gateuille et al., 2014, 2020).

7. CONCLUSIONS

We compared contamination levels in the large river basins using particulate micropollutant yields, which were explored through a bottom-up multiscale river basins approach. In this

respect, we compared micropollutant yields based on a unique dataset from a 10-year-long-monitoring program on the Rhône River sub-basins, then extrapolated up this approach to other major river basins in order to assess the spatial representativeness of this chemical contamination proxy.

Our reconstructions of the temporal trends of particulate micropollutant concentrations and fluxes at the Rhône River outlet since the 1980s show that micropollutant concentrations have to vary by more than 30% over 10 years to affect micropollutant fluxes. As a result, this threshold defines the tipping point marking the switch from SPM flux-driven to anthropogenic pressure-driven micropollutant yields. Applied to the other 18 large river basins worldwide, this balance between micropollutant concentrations and SPM fluxes suggests a progressive anthropogenic origin of the micropollutant yields as follows: (i) SPM flux-driven Co, Cr, Ni and Cu yields, (ii) anthropogenic activity and SPM flux-driven As, Zn and Pb yields, and (iii) anthropogenic activity-driven PCB, PAH, Cd and Hg yields. The distribution of the magnitude of chemical contamination in the large river basins is related to the economic development stage of the local country. Our results show an overall contamination gradient splitting the most contaminated river basins in developing and industrializing low-income and middle-income countries (Asia and South America) from the least contaminated rivers in developed high-income countries (Europe and North America). This kind of spatial pattern in surface waters-related chemical contamination fits well with the Environmental Kuznets Curve theory. Indeed, our results show how a prevailing model of economic development implies rampant urbanization supported by both increasingly high energy and natural resource consumption. In turn, these conditions constitute major sources of chemical contamination in the world's large river basins. In this respect, the long-term trend of contamination in the Rhône River basin shows an overall chemical contamination level in the 1980s that was similar to levels observed today in countries undergoing economic transition (Asia and South America). Then, starting in

the 1980s, chemical contamination levels of the Rhône River basin decreased, like the river basins in other developed countries, leading to improvement in water quality.

Large river monitoring is needed worldwide, with a special focus on river outlets and sustained monitoring for accurate global-level assessment of chemical contamination. In addition to the legacy micropollutants investigated in the present study, we also need to consider emerging chemicals (e.g. persistent mobile toxic substances), some of which need to be monitored in the dissolved fraction. Finally, we feel that there is a need for consistent data on geochemical background levels of TME for all of the world's large river basins, which would help to get a sharper picture of anthropogenic TME-related river basin contamination. All of these future developments could be implemented into watershed management plans to produce a standard of proof required to conclude that the EKC theory is indeed a correct explanation of the observed trends and could therefore be used to predict watershed trends worldwide.

ACKNOWLEDGMENTS

This study was conducted within the Rhône Sediment Observatory (OSR), a multi-partner research program funded through the Plan Rhône by the European Regional Development Fund (ERDF), Agence de l'eau RMC, CNR, EDF, and three French regional councils (Auvergne-Rhône-Alpes, PACA, and Occitanie). We are grateful to the INRAE colleagues Alexandra Gruat, Ghislaine Grisot, Mickaël Lagouy, Jérôme Le Coz, Aymeric Dabrin and Laurent Valette for their assistance with SPM sampling, field campaigns, sample treatment, chemical analysis, data analysis, and GIS analysis. We also thank Julie Gattacceca from the CEREGE laboratory, and Hugo Lepage and Olivier Radakovitch from the IRSN laboratory for coordinating the SPM sampling for the southern Rhône River stations and the ETM analyses (except Hg). Finally, we wish to thank the four anonymous reviewers and Stephen Sebestyen, guest editor, for greatly improving the manuscript.

REFERENCES

AERMC. 2019. Tableau de bord du SDAGE Rhône-Méditerranée 2016-2021 : bilan à mi-parcours (in French). Available at: https://www.eaurmc.fr/jcms/pro_95600/fr/tableau-de-bord-du-sdage-rhone-mediterranee-2016-2021-bilan-a-mi-parcours [Accessed on 18 August 2020]

Antonelli C, Eyrolle F, Rolland B, Provansal M, Sabatier F. 2008. Suspended sediment and 137Cs fluxes during the exceptional December 2003 flood in the Rhone River, southeast France. *Geomorphology* **95** (3): 350–360

Babut M, Persat H, Desmet M, Lopes, Mourier B, Tronczynski J. 2016. Les PCB dans le Rhône. In: *PCB, Environnement et Santé,* Paris; 473–498.

Bégorre C, Dabrin A, Morereau A, Lepage H, Mourier B, Masson M, Eyrolle F, Coquery M. 2021. Relevance of using the non-reactive geochemical signature in sediment core to estimate historical tributary contributions. *Journal of Environmental Management* **292**: 112775

Beketov MA, Kefford BJ, Schäfer RB, Liess M. 2013. Pesticides reduce regional biodiversity of stream invertebrates. *Proceedings of the National Academy of Sciences* **110** (27): 11039–11043

Best J. 2019. Anthropogenic stresses on the world's big rivers. *Nature Geoscience* **12** (1): 7–21

Bird G. 2011. Provenancing anthropogenic Pb within the fluvial environment: Developments and challenges in the use of Pb isotopes. *Environment International* **37** (4): 802–819

Blichert-Toft J, Delile H, Lee C-T, Stos-Gale Z, Billström K, Andersen T, Hannu H, Albarède F. 2016. Large-scale tectonic cycles in Europe revealed by distinct Pb isotope provinces. *Geochemistry, Geophysics, Geosystems* **17** (10): 3854–3864

Bravard J.-P 2018. *Crises sédimentaires du globe. 1, Grands cours d'eau, de l'abondance à la rareté*. ISTE éditions: London (in French).

Bravard, J-P, Clemens, A. 2008. *Le Rhône en 100 questions*. Zone Atelier Bassin du Rhône (ZABR), Villeurbanne, France (in French) ; 295 p

Breivik K, Sweetman A, Pacyna JM, Jones KC. 2002a. Towards a global historical emission inventory for selected PCB congeners — a mass balance approach: 1. Global production and consumption. *Science of The Total Environment* **290** (1): 181–198

Breivik K, Sweetman A, Pacyna JM, Jones KC. 2002b. Towards a global historical emission inventory for selected PCB congeners — a mass balance approach: 2. Emissions. *Science of The Total Environment* **290** (1): 199–224

Breivik K, Sweetman A, Pacyna JM, Jones KC. 2007. Towards a global historical emission inventory for selected PCB congeners — A mass balance approach: 3. An update. *Science of The Total Environment* **377** (2): 296–307

Cohen S, Kettner AJ, Syvitski JPM. 2014. Global suspended sediment and water discharge dynamics between 1960 and 2010: Continental trends and intra-basin sensitivity. *Global and Planetary Change* **115**: 44–58

Cohen S, Kettner AJ, Syvitski JPM, Fekete BM. 2013. WBMsed, a distributed global-scale riverine sediment flux model: Model description and validation. *Computers & geosciences* **53**: 80–93

Cornwall W. 2020. A dam big problem. *Science* **369** (6506): 906–909

Croiset N, Lopez B. 2013. HYPE : Outil d'analyse statistique des séries temporelles d'évolution de la qualité des eaux souterraines HYPE : Outil d'analyse statistique des séries temporelles d'évolution de la qualité des eaux souterraines. Manuel d'utilisation RP-63066-FR. BRGM (in French). http://infoterre.brgm.fr/rapports/RP-63066-FR.pdf

Dabrin A, Bégorre C, Bretier M, Dugué V, Masson M, Le Bescond C, Le Coz J, Coquery M. 2021. Reactivity of particulate element concentrations: apportionment assessment of suspended particulate matter sources in the Upper Rhône River, France. *Journal of*

Soils and Sediments **21**: 1256-1274

Damania R, Desbureaux S, Rodella A-S, Russ J, Zaveri E. 2019. *Quality Unknown : The Invisible Water Crisis*. Washington, DC: World Bank.

Darken P.F. (1999). Testing for changes in trend in water quality data. PhD Faculty of Virginia Polytehcnic Institute and State University.

Darken PF, Holtzman GI, Smith EP, Zipper CE. 2000. Detecting changes in trends in water quality using modified Kendall's tau. *Environmetrics* **11**: 423-434

Delile H, Masson M, Miège C, Le Coz J, Poulier G, Le Bescond C, Radakovitch O, Coquery M. 2020. Hydro-climatic drivers of land-based organic and inorganic particulate micropollutant fluxes: The regime of the largest river water inflow of the Mediterranean Sea. *Water Research* **185**: 116067

Dendievel A-M, Mourier B, Coynel A, Evrard O, Labadie P, Ayrault S, Debret M, Koltalo F, Copard Y, Faivre Q, et al. 2020a. Spatio-temporal assessment of the PCB sediment contamination in the four main French River Basins (1945-2018). Earth System Science Data Discussions: 1–23

Dendievel A-M, Mourier B, Dabrin A, Delile H, Coynel A, Gosset A, Liber Y, Berger J-F, Bedell J-P. 2020b. Metal pollution trajectories and mixture risk assessed by combining dated cores and subsurface sediments along a major European river (Rhône River, France). *Environment International* **144**: 106032

Dendievel A-M, Mourier B, Dabrin A, Barra A, Bégorre C, Delile H, Hammada M, Lardaux G, Berger J-F. 2020c. Dataset of natural metal background levels inferred from pre-industrial palaeochannel sediment cores along the Rhône River (France). *Data in Brief* **32**: 106256

Desforges J-P, Hall A, McConnell B, Rosing-Asvid A, Barber JL, Brownlow A, De Guise S, Eulaers I, Jepson PD, Letcher RJ, et al. 2018. Predicting global killer whale population

collapse from PCB pollution. *Science* **361** (6409): 1373–1376

Desmet M, Mourier B, Mahler BJ, Van Metre PC, Roux G, Persat H, Lefèvre I, Peretti A, Chapron E, Simonneau A, et al. 2012. Spatial and temporal trends in PCBs in sediment along the lower Rhône River, France. *Science of The Total Environment* **433**: 189–197

Dinda S. 2004. Environmental Kuznets Curve Hypothesis: A Survey. *Ecological Economics* **49** (4): 431–455

European Environment Agency (EEA), 2020. Corine Land Cover (CLC) 2018, v. 2020_20u1. URL: https://land.copernicus.eu/pan-european/corine-land-cover/clc2018

Eschbach D, Schmitt L, Imfeld G, May J-H, Payraudeau S, Preusser F, Trauerstein M, Skupinski G. 2018. Long-term temporal trajectories to enhance restoration efficiency and sustainability on large rivers: an interdisciplinary study. *Hydrology and Earth System Sciences* **22** (5): 2717–2737

Fostier AH, Forti MC, Guimarães JR, Melfi AJ, Boulet R, Espirito Santo CM, Krug FJ. 2000. Mercury fluxes in a natural forested Amazonian catchment (Serra do Navio, Amapá State, Brazil). *The Science of the Total Environment* **260** (1–3): 201–211

Förstner U, Heise S, Schwartz R, Westrich B, Ahlf W. 2004. Historical Contaminated Sediments and Soils at the River Basin Scale. *Journal of Soils and Sediments* **4** (4): 247

Gateuille D, Evrard O, Lefevre I, Moreau-Guigon E, Alliot F, Chevreuil M, Mouchel J-M. 2014. Mass balance and decontamination times of Polycyclic Aromatic Hydrocarbons in rural nested catchments of an early industrialized region (Seine River basin, France). *Science of The Total Environment* **470–471**: 608–617

Gateuille D, Gasperi J, Briand C, Moreau-Guigon E, Alliot F, Blanchard M, Teil M-J, Chevreuil M, Rocher V, Azimi S, et al. 2020. Mass Balance of PAHs at the Scale of the Seine River Basin. In: Flipo N., Labadie P., Lestel L. (eds) *The Seine River Basin*.

The Handbook of Environmental Chemistry, vol 90: 163–188

Gioia R, Dachs J, Nizzetto L, Berrojalbiz N, Galba C, Del Vento S, Méjanelle L, Jones KC. 2011. Sources, Transport and Fate of Organic Pollutants in the Oceanic Environment. In *Persistent Pollution – Past, Present and Future.* M. Quante, R. Ebinghaus, G. Flöser. Springer Berlin Heidelberg, 111–139.

Gómez-Gutiérrez AI, Jover E, Bodineau L, Albaigés J, Bayona JM. 2006. Organic contaminant loads into the Western Mediterranean Sea: estimate of Ebro River inputs. *Chemosphere* **65** (2): 224–236

Grossman, GM, & Krueger, AB 1991. Environmental impacts of a North American Free Trade Agreement. National Bureau of Economic Research Working Paper 3914, NBER, Cambridge MA. https://www.nber.org/papers/w3914

Grossman, GM, & Krueger, AB 1995. Economic Growth and the Environment. The *Quarterly Journal of Economics* **110** (2): 353–377

Hackney CR, Darby SE, Parsons DR, Leyland J, Best JL, Aalto R, Nicholas AP, Houseago RC. 2020. River bank instability from unsustainable sand mining in the lower Mekong River. *Nature Sustainability* **3** (3): 217–225

Hamed KH & Rao AR, 1998. A modified Mann-Kendall trend test for autocorrelated data. *Journal of Hydrology* **204** (1-4): 182-196

Heise S, Förstner U, Westrich B, Jancke T, Karnahl J, Salomons W, Schönberger H. 2004. Inventory of historical contaminated sediment in Rhine Basin and its tributaries. Report on Behalf of the Port of Rotterdam, p. 223

Immerzeel WW, Bierkens MFP. 2012. Asia's water balance. *Nature Geoscience* **5**: 841–842

INERIS. 2005. Hydrocarbures Aromatiques Polycycliques. Guide méthodologique. Acquisition des données d'entrée des modèles analytiques ou numériques de transferts dans les sols et les eaux souterraines. DRC – 66244 – DESP – R01 (in French).

INSEE. The National Institute of Statistics and Economic Studies Available at: https://www.insee.fr/fr/accueil [Accessed on 8 October 2020] (in French)

Kammerer JC. 1990. Largest rivers in the United States. Report 87–242. USGS, Department of the interior.

Kettner AJ, Syvitski JPM. 2008. HydroTrend v.3.0: A climate-driven hydrological transport model that simulates discharge and sediment load leaving a river system. *Computers & Geosciences* **34** (10): 1170–1183

Kubier A, Wilkin RT, Pichler T. 2019. Cadmium in soils and groundwater: A review. *Applied Geochemistry* **108**: 104388

Lacerda LD de, Salomons W. 1998. Mercury from gold and silver mining: a chemical time bomb? Springer: Berlin, New York.

Lade SJ, Steffen W, de Vries W, Carpenter SR, Donges JF, Gerten D, Hoff H, Newbold T, Richardson K, Rockström J. 2020. Human impacts on planetary boundaries amplified by Earth system interactions. *Nature Sustainability* **3** (2): 119–128

Landrigan PJ, Fuller R, Acosta NJR, Adeyi O, Arnold R, Basu N (Nil), Baldé AB, Bertollini R, Bose-O'Reilly S, Boufford JI, et al. 2018. The Lancet Commission on pollution and health. *The Lancet* **391** (10119): 462–512

Lauby-Secretan B, Loomis D, Grosse Y, El Ghissassi F, Bouvard V, Benbrahim-Tallaa L, Guha N, Baan R, Mattock H, Straif K, et al. 2013. Carcinogenicity of polychlorinated biphenyls and polybrominated biphenyls. *The Lancet. Oncology* **14** (4): 287–288

Le Bescond C, Thollet F, Poulier G, Gairoard S, Lepage H, Branger F, Jamet L, Raidelet N, Radakovitch O, Dabrin A, et al. 2018. Des flux d'eau aux flux de matières en suspension et de contaminants associés : gestion d'un réseau de stations hydro-sédimentaires sur le Rhône. *La Houille Blanche* (3): 63–70 (in French).

Legrand M, McConnell JR, Lestel L, Preunkert S, Arienzo M, Chellman NJ, Stohl A, Eckhardt

S. 2020. Cadmium pollution from zinc-smelters up to fourfold higher than expected in Western Europe in the 1980s as Revealed by Alpine Ice. *Geophysical Research Letters* **47** (10): e2020GL087537

Lehner B, Liermann CR, Revenga C, Vörösmarty C, Fekete B, Crouzet P, Döll P, Endejan M, Frenken K, Magome J, et al. 2011. High-resolution mapping of the world's reservoirs and dams for sustainable river-flow management. *Frontiers in Ecology and the Environment* **9** (9): 494–502

Liber Y, Mourier B, Marchand P, Bichon E, Perrodin Y, Bedell J-P. 2019. Past and recent state of sediment contamination by persistent organic pollutants (POPs) in the Rhône River: Overview of ecotoxicological implications. *Science of The Total Environment* **646**: 1037–1046

Liu K-K, Seitzinger S, Mayorga E, Harrison J, Ittekkot V. 2009. Fluxes of nutrients and selected organic pollutants carried by Rivers. In *Watersheds, bays and bounded Seas: the science and management of semi-enclosed marine systems.* Urban, E. R., Sundby, B., Malanotte-Rizzoli, P., and Melillo, J.: Island Press, Washington, DC; 141–167.

LUCRPO, LPSRIEP and Montgomery Watson 2001, Environmental Impact Assessment Report for the Liao River Basin Project, Liaoning Urban Construction and Renewal Project Office, Liaoning Provincial Scientific Research Institute for Environmental Projection and Montgomery Watson. E430, Vol 1, viewed 17 November 2020, http://info.worldbank.org/etools/docs/library/39794/Sample-EAreportLiaoRiverBasinProjectEN.pdf. [Accessed on 22 September 2020].

Ludwig W, Dumont E, Meybeck M, Heussner S. 2009. River discharges of water and nutrients to the Mediterranean and Black Sea: Major drivers for ecosystem changes during past and future decades? *Progress in Oceanography* **80** (3): 199–217

Macklin MG, Lewin J. 2015. The rivers of civilization. *Quaternary Science Reviews* **114**: 228–

244

Mai B, Zeng EY, Luo X, Yang Q, Zhang G, Li X, Sheng G, Fu J. 2005. Abundances, depositional fluxes, and homologue patterns of polychlorinated biphenyls in dated sediment cores from the Pearl River Delta, China. *Environmental Science & Technology* **39** (1): 49–56

Mäkelä A, Meybeck M. 1996. Designing a monitoring programme. In *Water Quality Monitoring : A Practical Guide to the Design and Implementation of Freshwater Quality Studies and Monitoring Programs*, Bartram J, Ballance R (eds). London: E & FN Spon; 37–59.

Malaj E, Ohe PC von der, Grote M, Kühne R, Mondy CP, Usseglio-Polatera P, Brack W, Schäfer RB. 2014. Organic chemicals jeopardize the health of freshwater ecosystems on the continental scale. *Proceedings of the National Academy of Sciences* **111** (26): 9549–9554

Masson M. 2007. Sources et transferts métalliques dans le bassin versant de la Gironde: Réactivité et mécanismes géochimiques dans l'estuaire fluvial de la Gironde. PhD Thesis, Bordeaux-I University.

Masson M, Angot H, Le Bescond C, Launay M, Dabrin A, Miège C, Le Coz J, Coquery M. 2018. Sampling of suspended particulate matter using particle traps in the Rhône River: Relevance and representativeness for the monitoring of contaminants. *The Science of the Total Environment* **637–638**: 538–549

McConnell JR, Chellman NJ, Wilson AI, Stohl A, Arienzo MM, Eckhardt S, Fritzsche D, Kipfstuhl S, Opel T, Place PF, Steffensen JP, 2019. Pervasive Arctic lead pollution suggests substantial growth in medieval silver production modulated by plague, climate, and conflict. *PNAS* **116** (30): 14910–14915

Meybeck M. 2003. Global analysis of river systems: from Earth system controls to

Anthropocene syndromes. *Philosophical Transactions of the Royal Society B: Biological Sciences* **358** (1440): 1935–1955

Meybeck M, Helmer R. 1989. The quality of rivers: From pristine stage to global pollution. *Palaeogeography, Palaeoclimatology, Palaeoecology* **75** (4): 283–309

Miller JR, Orbock Miller SM. 2007. Contaminated rivers: a geomorphological-geochemical approach to site assessment and remediation. Springer: Dordrecht, Pays-Bas.Mourier B, Desmet M, Van Metre PC, Mahler BJ, Perrodin Y, Roux G, Bedell J-P, Lefèvre I, Babut M. 2014. Historical records, sources, and spatial trends of PCBs along the Rhône River (France). *The Science of the Total Environment* **476–477**: 568–576

Mouyen M, Longuevergne L, Steer P, Crave A, Lemoine J-M, Save H, Robin C. 2018. Assessing modern river sediment discharge to the ocean using satellite gravimetry. *Nature Communications* **9** (1): 3384

Nienhuis JH, Ashton AD, Edmonds DA, Hoitink AJF, Kettner AJ, Rowland JC, Törnqvist TE. 2020. Global-scale human impact on delta morphology has led to net land area gain. *Nature* **577** (7791): 514–518

Nowak KC. 2011. Stochastic Streamflow Simulation at Interdecadal Times Scales and Implications for Water Resources Management in the Colorado River Basin. PhD Thesis, University of Colorado.

Noyes PD, McElwee MK, Miller HD, Clark BW, Van Tiem LA, Walcott KC, Erwin KN, Levin ED. 2009. The toxicology of climate change: environmental contaminants in a warming world. *Environment International* **35** (6): 971–986

Pacyna JM, Pacyna EG. 2001. An assessment of global and regional emissions of trace metals to the atmosphere from anthropogenic sources worldwide. *Environmental Reviews*: 269–298

Panayotou T. 2000. Economic Growth and the Environment. *CID Working Paper Series* **56**:

119

Pardé M. 1925. Le régime du Rhône. *Revue de Géographie Alpine* **13** (3): 459–547 (in French).

Pettitt A.N. (1979). A non-parametric approach to the change-point problem. Applied Statistics 28, 126-135.

Pfeiffer WC, Lacerda LD, Salomons W, Malm O. 1993. Environmental fate of mercury from gold mining in the Brazilian Amazon. *Environmental Reviews*: 26–37

Pizzuto J.E. 2014. Long-term storage and transport length scale of fine sediment: Analysis of a mercury release into a river. *Geophysical Research Letters* **41** (16): 5875–5882

Poulier G, Launay M, Le Bescond C, Thollet F, Coquery M, Le Coz J. 2019. Combining flux monitoring and data reconstruction to establish annual budgets of suspended particulate matter, mercury and PCB in the Rhône River from Lake Geneva to the Mediterranean Sea. *The Science of the Total Environment* **658**: 457–473

Qi W, Müller B, Pernet-Coudrier B, Singer H, Liu H, Qu J, Berg M. 2014. Organic micropollutants in the Yangtze River: Seasonal occurrence and annual loads. *Science of The Total Environment* **472**: 789–799

Rasmussen JJ, Wiberg-Larsen P, Baattrup-Pedersen A, Monberg RJ, Kronvang B. 2012. Impacts of pesticides and natural stressors on leaf litter decomposition in agricultural streams. *The Science of the Total Environment* **416**: 148–155

Rockström J, Steffen W, Noone K, Persson A, Chapin FS, Lambin EF, Lenton TM, Scheffer M, Folke C, Schellnhuber HJ, et al. 2009. A safe operating space for humanity. *Nature* **461** (7263): 472–475

Roulet M, Lucotte M, Farella N, Serique G, Coelho H, Sousa Passos C, de Jesus da Silva E, Scavone de Andrade P, Mergler D, Guimarães J-RD, et al. 1999. Effects of Recent Human Colonization on the Presence of Mercury in Amazonian Ecosystems |

SpringerLink. *Water, Air, and Soil Pollution* **112**: 297–313

Rügner H, Schwientek M, Milačič R, Zuliani T, Vidmar J, Paunović M, Laschou S, Kalogianni E, Skoulikidis NT, Diamantini E, et al. 2019. Particle bound pollutants in rivers: Results from suspended sediment sampling in Globaqua River Basins. *The Science of the Total Environment* **647**: 645–652

Sartorius C, Hillenbrand T, Walz R. 2011. Impact and cost of measures to reduce nutrient emissions from wastewater and storm water treatment in the German Elbe river basin. *Regional Environmental Change* **11**: 377–391

Schäfer RB, Gerner N, Kefford BJ, Rasmussen JJ, Beketov MA, de Zwart D, Liess M, von der Ohe PC. 2013. How to characterize chemical exposure to predict ecologic effects on aquatic communities? *Environmental Science & Technology* **47** (14): 7996–8004

Scheurle C, Hebbeln D, Jones P. 2005. An 800-year reconstruction of Elbe River discharge and German Bight sea-surface salinity. *The Holocene* **15** (3): 429–434

Schulze T, Ricking M, Schröter-Kermani C, Körner A, Denner H-D, Weinfurtner K, Winkler A, Pekdeger A. 2007. The German Environmental Specimen Bank. *Journal of Soils and Sediments* **7** (6): 361–367

Schwarzenbach RP, Egli T, Hofstetter TB, von Gunten U, Wehrli B. 2010. Global Water Pollution and Human Health. *Annual Review of Environment and Resources* **35** (1): 109–136

Schwarzenbach RP, Escher BI, Fenner K, Hofstetter TB, Johnson CA, Gunten U von, Wehrli B. 2006. The Challenge of Micropollutants in Aquatic Systems. *Science* **313** (5790): 1072–1077

Schwientek M, Rügner H, Beckingham B, Kuch B, Grathwohl P. 2013. Integrated monitoring of particle associated transport of PAHs in contrasting catchments. *Environmental Pollution* **172**: 155–162

Shafik N. 1994. Economic Development and Environmental Quality: An Econometric Analysis. *Oxford Economic Papers* **46** (Special Issue on Environmental Economics): 757–773

Shafik, N., Bandyopadhyay, S. 1992. Economic Growth and Environmental Quality: Time-Series and Cross-Country Evidence. Background Paper for the World Development Report. The World Bank, Washington, DC.

Shen H, Huang Y, Wang R, Zhu D, Li W, Shen G, Wang B, Zhang Y, Chen Y, Lu Y, et al. 2013. Global atmospheric emissions of polycyclic aromatic hydrocarbons from 1960 to 2008 and future predictions. *Environmental science & technology* **47** (12): 6415–6424

Shen H, Tao S, Wang R, Wang B, Shen G, Li W, Su S, Huang Y, Wang X, Liu W, et al. 2011. Global time trends in PAH emissions from motor vehicles. *Atmospheric Environment* **45** (12): 2067–2073

Singer MB, Aalto R, James LA, Kilham NE, Higson JL, Ghoshal S. 2013. Enduring legacy of a toxic fan via episodic redistribution of California gold mining debris. *Proceedings of the National Academy of Sciences* **110** (46): 18436–18441

Steffen W, Richardson K, Rockström J, Cornell SE, Fetzer I, Bennett EM, Biggs R, Carpenter SR, de Vries W, de Wit CA, et al. 2015. Sustainability. Planetary boundaries: guiding human development on a changing planet. *Science* **347** (6223): 736–746

Stern DI. 2004. The Rise and Fall of the Environmental Kuznets Curve. *World Development* **32** (8): 1419–1439

Stern DI, Common MS, Barbier EB. 1996. Economic growth and environmental degradation: The environmental Kuznets curve and sustainable development. *World Development* **24** (7): 1151–1160

Stigliani WM. 1991. Chemical Time Bombs: Definition, Concepts, and Examples. Executive report 16. International institute for applied systems analysis, Laxenburg, Austria.

Streets DG, Horowitz HM, Jacob DJ, Lu Z, Levin L, ter Schure AFH, Sunderland EM. 2017. Total Mercury Released to the Environment by Human Activities. *Environmental Science & Technology* **51** (11): 5969–5977

Sutfin NA, Wohl E. 2019. Elevational differences in hydrogeomorphic disturbance regime influence sediment residence times within mountain river corridors. *Nature Communications* **10** (1): 2221

Syvitski JPM, Kettner AJ. 2007. On the flux of water and sediment into the Northern Adriatic Sea. *Continental Shelf Research* **27** (3): 296–308

Syvitski JPM, Vörösmarty CJ, Kettner AJ, Green P. 2005. Impact of humans on the flux of terrestrial sediment to the global coastal ocean. *Science* **308** (5720): 376–380

Syvitski PM, Kettner A. 2011. Sediment flux and the Anthropocene. *Philosophical Transactions of the Royal Society A: Mathematical, Physical and Engineering Sciences* **369** (1938): 957–975

Thollet F, Le Bescond C, Lagouy M, Gruat A, Grisot G, Le Coz J, Coquery M, Lepage H, Gairoard S, Gattacceca JC, Ambrosi J-P, Radakovitch O, Dur G, Richard L, Giner F, Eyrolle F, Angot H, Mourier D, Bonnefoy A, Dugué V, Launay M, Troudet L, Labille J, Kieffer L, 2021. Observatoire des Sédiments du Rhône. Irstea. Available at: https://dx.doi.org/10.17180/OBS.OSR

UNECE — United Nations Economic Commission for Europe. 1979 — European Environment Agency. The Geneva Convention on Long-range Transboundary Air Pollution. Nations Unies. Commission économique pour l'Europe, New-York. Available at: https://www.eea.europa.eu/data-and-maps/indicators/main-anthropogenic-air-pollutant-emissions/unece-1979 [Accessed on 20 November 2020]

UNEP — United Nations Environment Programme. 2001. Final Act of the Plenipotentiaries on the Stockholm Convention on Persistent Organic Pollutants. United Nations

Environment Program Chemicals, Geneva, Switzerland.

UNEP/MAP — United Nations Environment Programme — Mediterranean Action Plan. 2003. Riverine transport of water, sediments and pollutants to the Mediterranean Sea. Technical Reports 141. Athens.

UNEP-DHI and UNEP —- 2016. Transboundary River Basins: Status and Trends. United Nations Environment Programme (UNEP). Vol. 3: River basins, Nairobi.

UNESCO (ed.). 2009. *Water in a changing world*. UNESCO: Paris, London.

United Nations, 1998. Protocol to the 1979 convention on long-range transboundary air pollution on persistent organic pollutants. ECE/EB.AIR/ 60.

Vianello A. 2015. *Rivers in Prehistory*. Archaeopress.

Wang J-Z, Guan Y-F, Ni H-G, Luo X-L, Zeng EY. 2007. Polycyclic Aromatic Hydrocarbons in Riverine Runoff of the Pearl River Delta (China): Concentrations, Fluxes, and Fate. *Environmental Science & Technology* **41** (16): 5614–5619

Wilkinson P, Smith KR, Beevers S, Tonne C, Oreszczyn T. 2007. Energy, energy efficiency, and the built environment. *Lancet (London, England)* **370** (9593): 1175–1187

Wohl E. 2015. Legacy effects on sediments in river corridors. *Earth-Science Reviews* **147**: 30–53

Wohl E. 2019. Forgotten Legacies: Understanding and Mitigating Historical Human Alterations of River Corridors. *Water Resources Research* **55** (7): 5181–5201

World Bank national accounts data, and OECD National Accounts data files. https://data.worldbank.org/indicator/NY.GDP.MKTP.CD [Accessed on 10 October 2020].

World Cities Database. 2020. Creative Commons Attribution 4.0 license. Available at: https://simplemaps.com/data/world-cities [Accessed on 10 October 2020].

Xing Y, Lu Y, Liu W. 2011. Environmental Contamination Status of Polychlorinated

Biphenyls in China. In *Global Environmental Distribution and Human Health Effects of Polycyclic Aromatic Hydrocarbons*, Loganathan BG, Lam PKS (eds).CRC Press: Boca Raton (FL, USA); 163–177.

Xu S, Jiang X, Dong Y, Sun C, Feng J, Wang L, Martens D, Gawlik BM. 2000. Polychlorinated organic compounds in Yangtse River sediments. *Chemosphere* **41** (12): 1897–1903

Captions of the figures and tables

Figure 1. (A) Map of the Rhône River basin with its main tributaries and monitoring stations for water discharge, suspended particulate matter, and associated micropollutants. (B) Land-use distribution (in %) in the basin of the Rhône River (Arles/Beaucaire station) and its main tributaries.

Figure 2. Changes of $\sum_7$PCBi (A and B), $\sum_{12}$PAH (C and D) and TME (E and F) concentrations (µg or mg kg^{-1}) and fluxes (kg or t yr^{-1}) since the 1980s at the Rhône River outlet. The high-resolution temporal trend of micropollutant concentrations over the 2000–2010 period is detailed in Fig. 3. In panels A and B, the black arrow labeled "1975" indicates the year that PCBs were banned in closed devices (order of 8 July 1975), and the black arrow labeled "1987" indicates the year of the blanket ban on the same PCBs and the ban on the production of devices using PCBs at > 0.5 g kg^{-1} (decree 87-59).

Figure 3. High-resolution temporal trend of $\sum_7$PCBi, $\sum_{12}$PAH and TME concentrations (µg or mg kg^{-1}) from 2008 to 2019 at the Rhône River mouth (Arles/Beaucaire station). Blue histograms show mean monthly water discharges (m^3 s^{-1}) at the Rhône River outlet. Red dotted lines show the temporal trends in micropollutant concentration time-series (see § 4.1.1. for statistical treatment details); and red values indicate increasing or decreasing contamination rates (µg or mg kg^{-1} yr^{-1}), respectively, over the total length of the time-series. Green dotted lines indicate the trend change-point dates (see § 4.1.1. for statistical treatment details); and the green values indicate increasing or decreasing contamination rates before and after the change-

point dates (µg or mg kg^{-1} yr^{-1}). Only the temporally significant trends are shown (p-value < 0.05 for non-parametric Mann-Kendall tests).

Figure 4. Maps of the $\sum_{12}$PAH, $\sum_{5}$PCBi, TME and SPM yields in the Rhône River basin and its main sub-basins.

Figure 5. Principal Component Analysis (PCA) of all inter-annual micropollutant yields, land-use cover and population density for the monitoring stations on the Rhône River basin and at its outlet (Arles/Beaucaire station). See Supporting Text for details on PCA method used. The land-use classification used is the same as for Fig. 1B, i.e. "Agri" for agricultural lands, "Forests" for forest areas, "Bare" for bare areas, "Vegetal" for shrub and/or grassy vegetation, "ICA" for industrial and commercial areas, and "Urban" for urban areas. On the whole, the dominant factor F1 results from the contribution of all micropollutant (except for $\sum_{5}$PCBi) and SPM yields. Factor F2 opposes the anthropogenic-related land use categories (urban, agricultural, industrial and commercial areas) against the forests land-use category.

Figure 6. Maps of the $\sum_{12\text{-}16}$PAH, $\sum_{7}$PCBi, Hg, Cd and SPM yields, and GDP per capita in the major world river basins (1-Rhône, 2-Garonne, 3-Loire, 4-Seine, 5-Volga, 6-Danube, 7-Elbe, 8-Rhine, 9-Pearl (Zhujiang), 10-Liao, 11-Yangtze (Changjiang), 12-Yellow (Huang He), 13-Mekong, 14-Ganges-Brahmaputra, 15-Mississippi, 16-Colorado, 17-St. Lawrence, 18-Amazon, 19-Niger).

Figure 7. PCA of all micropollutant and SPM yields, density of dams, populations and cities, and GDP per capita in the major world river basins (see Supporting Text for details on the PCA). On the whole, the dominant factor F1 results from the contribution of a large share of micropollutant and SPM yields, and factor F2 is mostly driven by economic parameters (dams density, population density, cities density, and GDP per capita). Panel A shows the correlation circle in which three groups of micropollutant yields gather (gray ellipses) according to their correlations with SPM yields and median micropollutant concentrations (Fig. S2) (see

correlation coefficients and p-values in text and Tab. S3 and S4). Thus, groups 1, 2 and 3 are anthropogenic activity-driven micropollutant yields, SPM flux-driven micropollutant yields and anthropogenic activity/SPM flux-driven micropollutant yields, respectively. Panel B displays the observations plot defining three mixing lines (gray dotted lines) for overall contamination level from the least-contaminated river basins in the bottom-left corner of the graph up to the most-contaminated river basins in the upper-right part of the graph. Mixing lines were statistically defined as follows: linking the origin to the average F1 and F2 biplot loadings (gray crosses) across all 11 micropollutants (Groups 1 + 2 + 3-based mixing line), a set of 7 micropollutants (Groups 1 + 3-based mixing line) and a set of 4 micropollutants (Group 1-based mixing line). Slope angularity of the mixing lines thus gives the balance between the anthropogenic origin of the micropollutant yields (Group 1-based mixing line) and the weight of the SPM fluxes in the micropollutant yields (Groups 1 + 2 + 3-based mixing line). The black curved arrow shows the environmental quality improvement of the Rhône River basin since the 1980s.

Figure 8. Inter-annual micropollutant yields of the major river basins (Rhône, Garonne, Loire, Seine, Volga, Danube, Elbe, Rhine, Pearl (Zhujiang), Liao, Yangtze (Changjiang), Yellow (Huang He), Mekong, Ganges-Brahmaputra, Mississippi, Colorado, St. Lawrence, Amazon and Niger Rivers).

Table 1. Main physical and human characteristics of the large river basins investigated in this study. Data sources are shown in footnotes.

Table 2. River sediment matrices and data sources used to assess the temporal trends in particulate micropollutant concentrations and fluxes at the Rhône River outlet listed by micropollutant family and the decades considered.

Table 3. Long-term decadal variations (in %) in inter-annual particulate micropollutant concentrations (ΔC) and fluxes (ΔF) and SPM fluxes at the Rhône River outlet. Orange cells show the micropollutant flux variations that are mainly dependent on micropollutant concentration variations, while grey cells highlight micropollutant flux variations that are mainly dependent on SPM flux variations. The bottom part of the table shows the correlation coefficients for decadal micropollutant fluxes and concentrations (first line) and for micropollutant fluxes and SPM fluxes (second line).

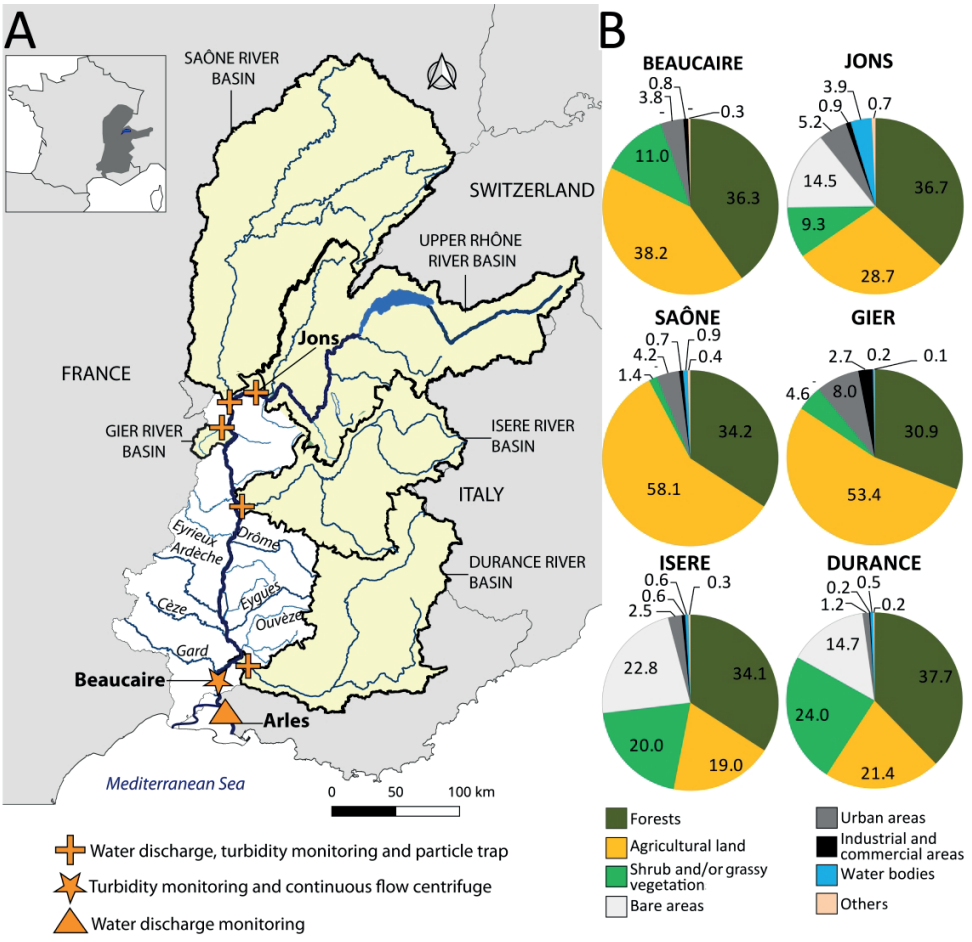

Figure 1. (A) Map of the Rhône River basin with its main tributaries and monitoring stations for water discharge, suspended particulate matter, and associated micropollutants. (B) Land-use distribution (in %) in the basin of the Rhône River (Arles/Beaucaire station) and its main tributaries.

299x288mm (400 x 400 DPI)

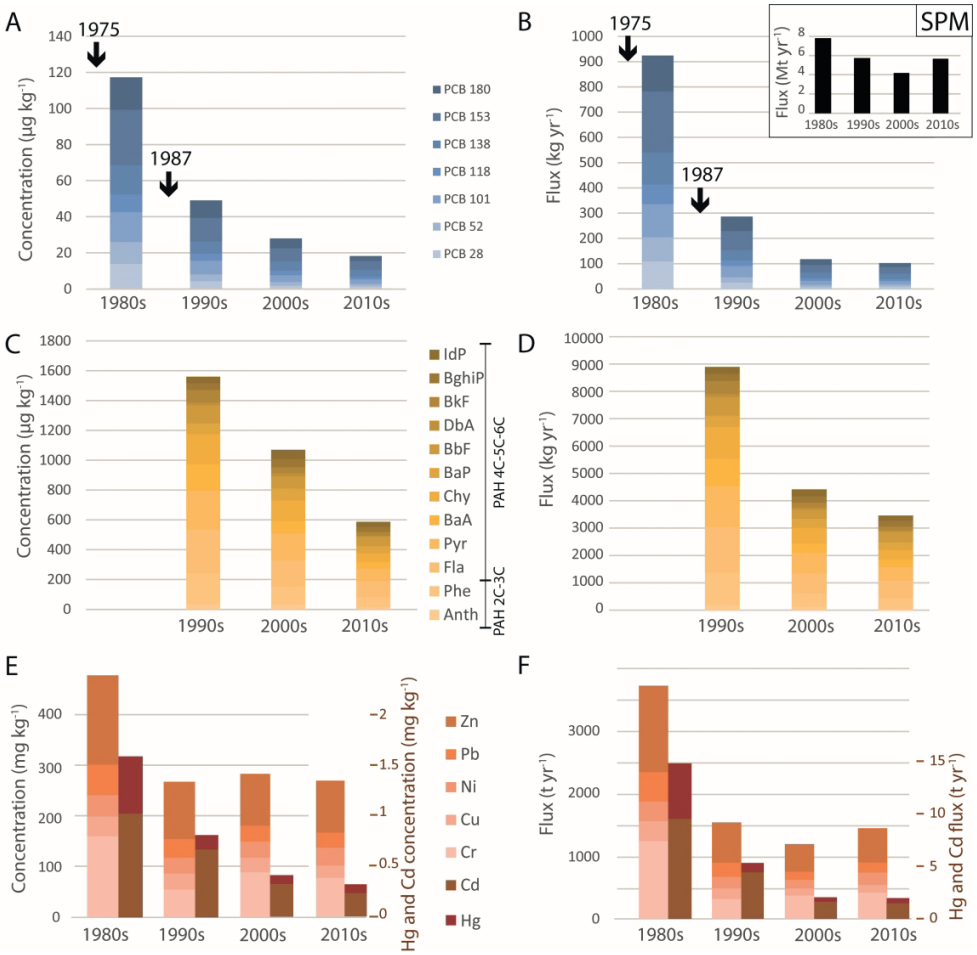

Figure 2. Changes of ∑7PCBi (A and B), ∑12PAH (C and D) and TME (E and F) concentrations (µg or mg kg-1) and ¬fluxes (kg or t yr-1) since the 1980s at the Rhône River outlet. The high-resolution temporal trend of micropollutant concentrations over the 2000–2010 period is detailed in Fig. 3. In panels A and B, the black arrow labeled "1975" indicates the year that PCBs were banned in closed devices (order of 8 July 1975), and the black arrow labeled "1987" indicates the year of the blanket ban on the same PCBs and the ban on the production of devices using PCBs at > 0.5 g kg-1 (decree 87-59).

196x191mm (600 x 600 DPI)

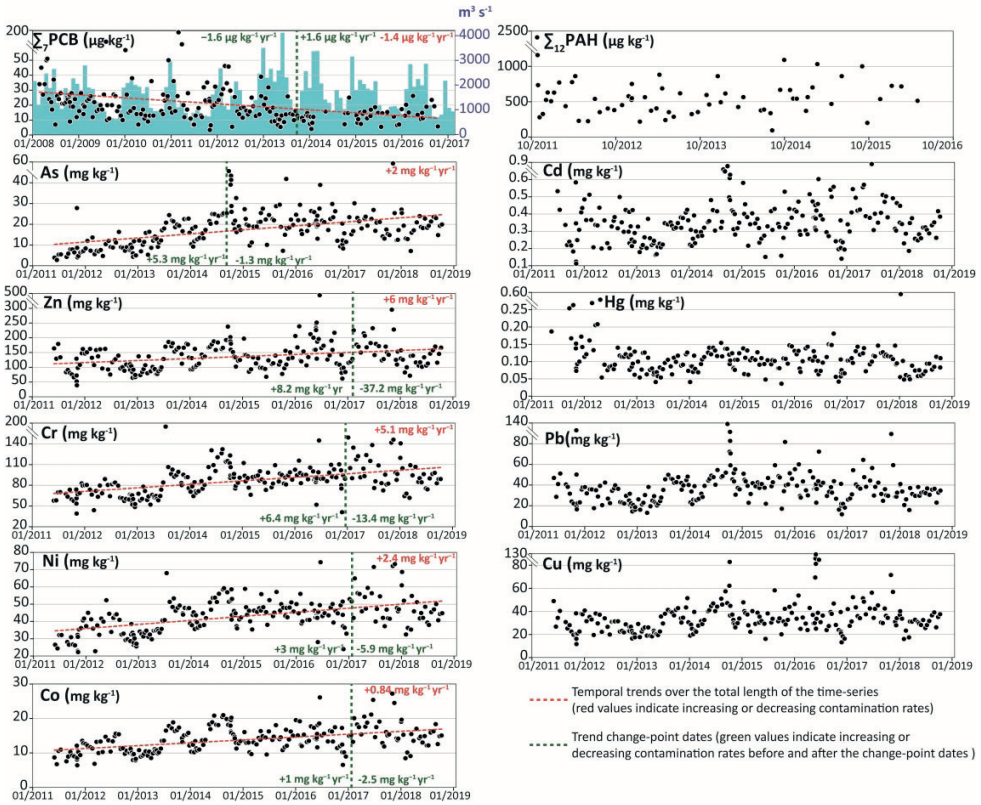

Figure 3. High-resolution temporal trend of ∑7PCBi, ∑12PAH and TME concentrations (µg or mg kg-1) from 2008 to 2019 at the Rhône River mouth (Arles/Beaucaire station). Blue histograms show mean monthly water discharges (m3 s-1) at the Rhône River outlet. Red dotted lines show the temporal trends in micropollutant concentration time-series (see § 4.1.1. for statistical treatment details); and red values indicate increasing or decreasing contamination rates (µg or mg kg-1 yr-1), respectively, over the total length of the time-series. Green dotted lines indicate the trend change-point dates (see § 4.1.1. for statistical treatment details); and the green values indicate increasing or decreasing contamination rates before and after the change-point dates (µg or mg kg-1 yr-1). Only the temporally significant trends are shown (p-value < 0.05 for non-parametric Mann-Kendall tests).

402x332mm (400 x 400 DPI)

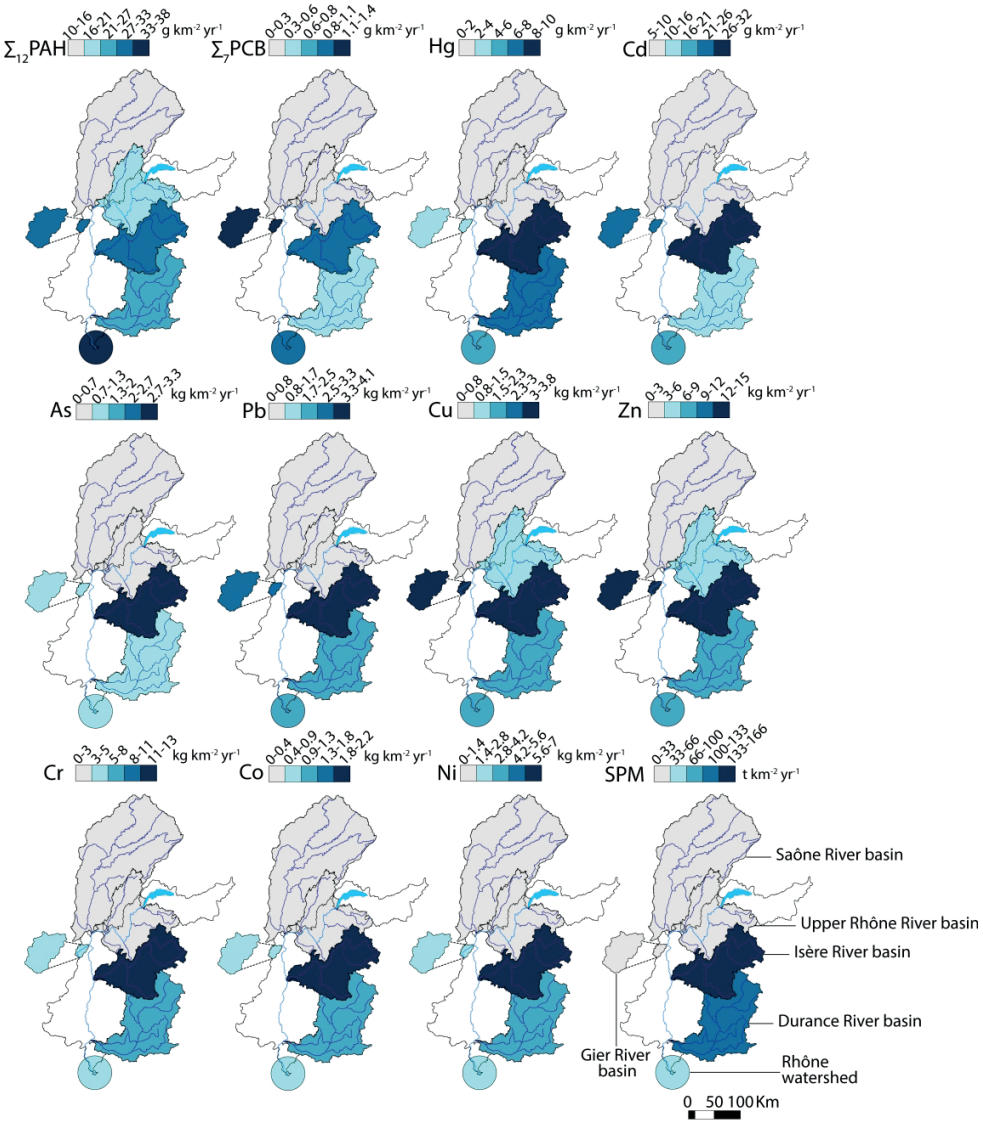

Figure 4. Maps of the Σ12PAH, Σ5PCBi, TME and SPM yields in the Rhône River basin and its main sub-basins.

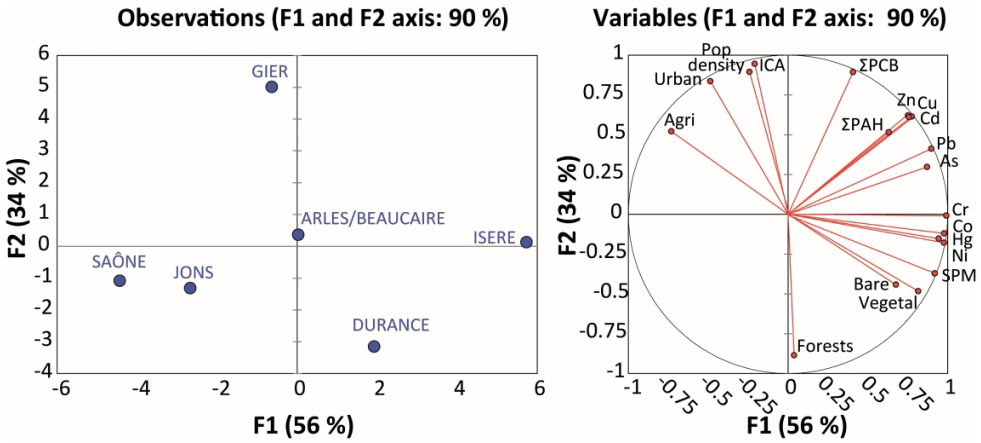

Figure 5. Principal Component Analysis (PCA) of all inter-annual micropollutant yields, land-use cover and population density for the monitoring stations on the Rhône River basin and at its outlet (Arles/Beaucaire station). See Supporting Text for details on PCA method used. The land-use classification used is the same as for Fig. 1B, i.e. "Agri" for agricultural lands, "Forests" for forest areas, "Bare" for bare areas, "Vegetal" for shrub and/or grassy vegetation, "ICA" for industrial and commercial areas, and "Urban" for urban areas. On the whole, the dominant factor F1 results from the contribution of all micropollutant (except for ∑5PCBi) and SPM yields. Factor F2 opposes the anthropogenic-related land use categories (urban, agricultural, industrial and commercial areas) against the forests land-use category.

178x80mm (600 x 600 DPI)

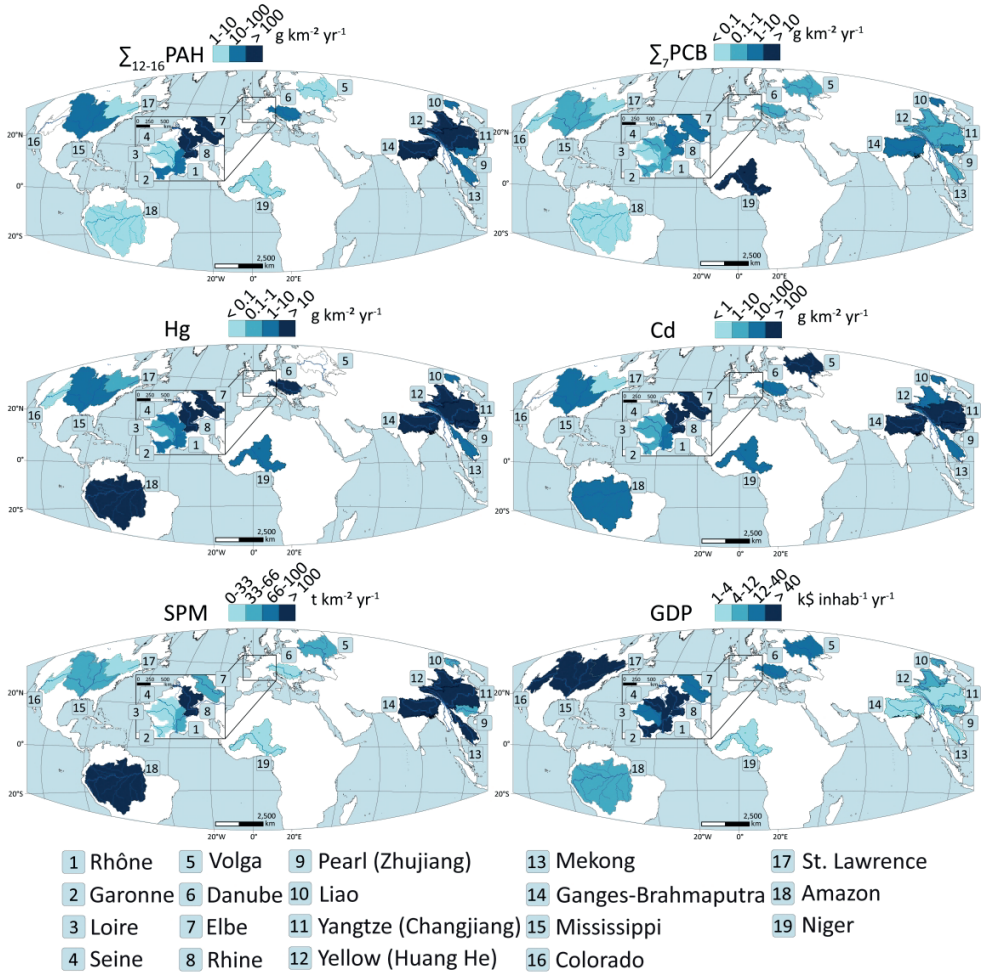

Figure 6. Maps of the Σ12-16PAH, Σ7PCBi, Hg, Cd and SPM yields, and GDP per capita in the major world river basins (1-Rhône, 2-Garonne, 3-Loire, 4-Seine, 5-Volga, 6-Danube, 7-Elbe, 8-Rhine, 9-Pearl (Zhujiang), 10-Liao, 11-Yangtze (Changjiang), 12-Yellow (Huang He), 13-Mekong, 14-Ganges-Brahmaputra, 15-Mississippi, 16-Colorado, 17-St. Lawrence, 18-Amazon, 19-Niger).

424x425mm (350 x 350 DPI)

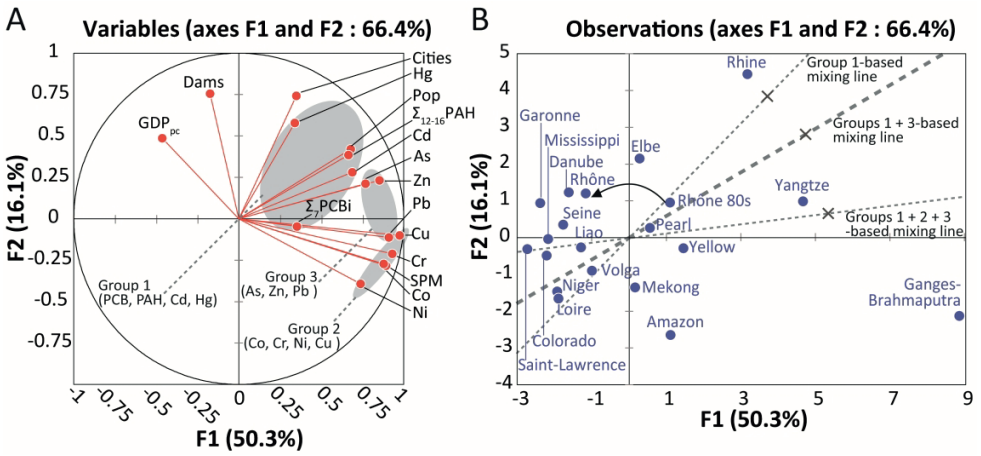

Figure 7. PCA of all micropollutant and SPM yields, density of dams, populations and cities, and GDP per capita in the major world river basins (see Supporting Text for details on the PCA). On the whole, the dominant factor F1 results from the contribution of a large share of micropollutant and SPM yields, and factor F2 is mostly driven by economic parameters (dams density, population density, cities density, and GDP per capita). Panel A shows the correlation circle in which three groups of micropollutant yields gather (gray ellipses) according to their correlations with SPM yields and median micropollutant concentrations (Fig. S2) (see correlation coefficients and p-values in text and Tab. S3 and S4). Thus, groups 1, 2 and 3 are anthropogenic activity-driven micropollutant yields, SPM flux-driven micropollutant yields and anthropogenic activity/SPM flux-driven micropollutant yields, respectively. Panel B displays the observations plot defining three mixing lines (gray dotted lines) for overall contamination level from the least-contaminated river basins in the bottom-left corner of the graph up to the most-contaminated river basins in the upper-right part of the graph. Mixing lines were statistically defined as follows: linking the origin to the average F1 and F2 biplot loadings (gray crosses) across all 11 micropollutants (Groups 1 + 2 + 3-based mixing line), a set of 7 micropollutants (Groups 1 + 3-based mixing line) and a set of 4 micropollutants (Group 1-based mixing line). Slope angularity of the mixing lines thus gives the balance between the anthropogenic origin of the micropollutant yields (Group 1-based mixing line) and the weight of the SPM fluxes in the micropollutant yields (Groups 1 + 2 + 3-based mixing line). The black curved arrow shows the environmental quality improvement of the Rhône River basin since the 1980s.

192x89mm (600 x 600 DPI)

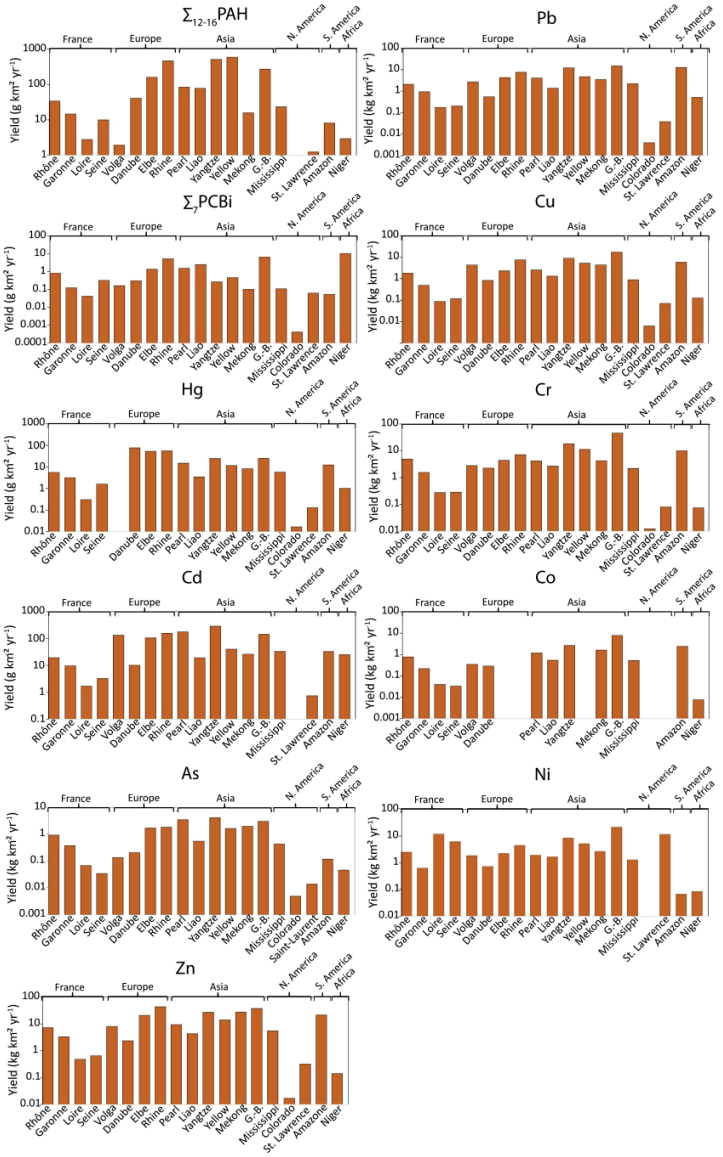

Figure 8. Inter-annual micropollutant yields of the major river basins (Rhône, Garonne, Loire, Seine, Volga, Danube, Elbe, Rhine, Pearl (Zhujiang), Liao, Yangtze (Changjiang), Yellow (Huang He), Mekong, Ganges-Brahmaputra, Mississippi, Colorado, St. Lawrence, Amazon and Niger Rivers).

1223x1979mm (96 x 96 DPI)

	Lenght (km)	Watershed (km²)	Mean water discharge ($m^3 s^{-1}$)	SPM flux (Mt yr^{-1})	SPM yield (t $km^{-2} yr^{-1}$)	Population (M inhab)	Population density (inhab km^2)	Number of large cities (> 500 000)	Cities density (cities 10^5 km^2)	GDP (billion USD yr^{-1})	GDP per capita (USD yr^{-1})	Number of dams	Dams density (M km^2)
Rhône	765[1]	89 000[2]	1 620[3]	5.5[3]	63	15.5[4]	175	12[2]	14	642	41 421[2]	30[2]	337
Garonne	529[5]	51 257[5]	650[5]	1[5]	20	5.9[5]	115	2[2]	4	244	41 421[2]	24[2]	427
Loire	1006[5]	110 726[5]	870[5]	0.4[5]	3.8	14.3[5]	129	2[6]	2	451	31 555[6]	3[5]	27
Seine	775[5]	65 366[5]	600[5]	0.4[5]	6.5	20.1[5]	307	7[2]	11	833	41 421[2]	10[2]	136
Volga	3 692[7]	1 411 000[2]	8 103[7]	47.3[8]	33.5	58.6[2]	42	74[2]	5	857	14 612[2]	17[2]	12
Danube	2 900[7]	796 000[2]	6 659[7]	20.2[8]	25.4	80.2[2]	101	63[2]	8	1 482	18 478[2]	184[2]	231
Elbe	1 165[10]	148 268[9]	750[10]	7.9[8]	53.2	24.7[9]	167	16[2]	11	937	37 940[2]	42[2]	302
Rhine	1 400[7]	163 609[2]	2 347[7]	17.3[8]	105.8	48.8[2]	298	62[2]	38	2 419	49 543[2]	42[2]	257
Pearl (Zhujiang)	2 200[7]	490 000[7]	8 245[7]	25[8]	51	75[7]	153	40[2]	8	506	6 740[2]	49[2]	122
Liao	1 345[12]	229 000[12]	82[12]	9[12]	39.3	33[11]	144	20[13]	9	156[13]	4 716	41[14]	179
Yangtze (Changjiang)	6 300[7]	1 800 000[7]	28 538[7]	284[8]	157	601[15]	332	56[13]	3	1 796[13]	2 988	380[14]	210
Yellow (Huang He)	5 500[7]	750 000[7]	1 364[7]	120[8]	159	162[15]	215	36[13]	5	751[13]	4 636	48[14]	64
Mekong	4 800[7]	773 000[7]	17 440[7]	95[8]	122	59[2]	76	16[2]	2	226	3854[2]	20[2]	26
Mississippi	5 900[7]	3 208 000[7]	15 538[7]	132[8]	41	78.2[2]	24	54[2]	1.7	4 154	53 142[2]	707[2]	220
Colorado	2 330[16]	626 050[2]	640[17]	0.13[8]	0.2	8.8[2]	14	16[2]	2.5	456	51 802[2]	82[2]	131
Saint-Lawrence	4 000[7]	1 057 304[7]	10 781[7]	4.6[8]	4.4.	45.9[2]	43	37[2]	3.5	2 416	52 663[2]	176[2]	166
Niger	4 000[7]	2 111 475[7]	6 025[7]	25.2[8]	11.9	93.6[7]	44	33[2]	1.6	199	2 125[2]	56[2]	27
Amazon	6 300[7]	5 888 269[2]	199 772[7]	978[8]	166	32.2[2]	5.5	21[2]	0.4	225	6 998[2]	8[2]	1
Ganges-Brahmaputra	2 600[7]	1 652 367[2]	17 760[7]	1 104[8]	669	540.4[7]	327	194[2]	12	728	1 347[2]	82[2]	50

[1]Bravard & Clémens (2018)
[2]UNEP-DHI & UNEP (2016)
[3]Delile et al. (2020)
[4]AERMC (2019)
[5]Dendievel et al. (2020b)
[6]INSEE
[7]Best (2019)
[8]Nienhuis et al. (2020)
[9]Sartorius & Hillenbrand (2011)
[10]Scheurle et al. (2005)
[11]LUCRPO et al. (2001)
[12]Liu et al. (2013)
[13]World Bank
[14]Lehner et al. (2011)
[15]Immerzeel & Bierkens (2012)
[16]Kammerer (1990)
[17]Nowak (2011)

Micropollutants family	Studied periods	River sediment matrices	Data sources	References and availability
TME (Cd, Cr, Cu, Hg, Ni, Pb, Zn)	1980s-2010s	Bed and flood deposits, sediment cores, and SPM	Rhône–Mediterranean–Corsica water agency, OSR monitoring program, and research institutes	Dendievel et al., 2020a,b; Thollet et al., 2021; Delile et al., 2020.
TME (As, Cd, Co, Cr, Cu, Hg, Ni, Pb and Zn)	2011-2018	SPM	OSR monitoring program	Thollet et al., 2021; Delile et al., 2020.
PCBi (congeners 28, 52, 101, 118, 138, 153, and 180)	1980s-2010s	Bed and flood deposits, sediment cores, and SPM	Rhône–Mediterranean–Corsica water agency, OSR monitoring program, and research labs	Dendievel et al., 2020a,b; Thollet et al., 2021; Delile et al., 2020.
PCBi (congeners 28, 52, 101, 118, 138, 153, and 180)	2008-2017	SPM	OSR monitoring program	Thollet et al., 2021; Delile et al., 2020.
PAHs (Ant, BaA, BaP, BbF, BghiP, BkF, Chy, DbA, Fla, IdP, Phe, Pyr)	1990s-2010s	Bed and flood sediments, and SPM	Rhône–Mediterranean–Corsica water agency, OSR monitoring program	http://www.naiades.eaufrance.fr; Thollet et al., 2021; Delile et al., 2020.
PAHs (Ant, BaA, BaP, BbF, BghiP, BkF, Chy, DbA, Fla, IdP, Phe, Pyr)	2011-2016	SPM	OSR monitoring program	Thollet et al., 2021; Delile et al., 2020.

	$\sum_7$PCB		$\sum_{12}$PAH		Cd		Cr		Hg		Pb		Zn		Cu		Ni		Mean TME		SPM
	ΔC	ΔF	ΔC	ΔF	ΔC	ΔF	ΔC	ΔF	ΔC	ΔF	ΔC	ΔF	ΔC	ΔF	ΔC	ΔF	ΔC	ΔF	ΔC	ΔF	ΔF
1980s-1990s	-58	-69			-35	-52	-66	-75	-76	-83	-36	-53	-37	-53	-26	-45	-21	-41	-42	-57	-26
1990s-2000s	-43	-59	-31	-50	-54	-67	+63	+18	-35	-53	-21	-43	-6	-32	-7	-33	+2	-26	-8	-34	-28
2000s-2010s	-35	-15	-45	-20	-25	-3	-15	+12	-4	+38	-3	+26	-3	+25	-15	+9	+8	+42	-8	+21	+44
R $F_{micropol}$ vs. $C_{micropol}$	**1.00**		**0.94**		**0.99**		**0.97**		**1.00**		**0.99**		**0.99**		**0.96**		0.93				
R $F_{micropol}$ vs. F_{SPM}	0.92		0.24		0.93		0.87		0.92		**0.96**		**0.96**		**0.95**		**0.98**				

Correlations in bold for p value ≤ 0.05